The darkening of the Greenland ice sheet: trends, drivers and projections (1981 – 2100)

M. Tedesco[1,2], S. Doherty[3], X. Fettweis[4], P. Alexander[2,5,6], J. Jeyaratnam[2], and J. Stroeve[7]

[1] Lamont-Doherty Earth Observatory of the Columbia University, New York, NY

[2] The City College of New York – CUNY,

[3] Joint Institute for the Study of the Atmosphere and Ocean (JISAO), University of Washington, Seattle, WA USA

[4] University of Liege, Liege, Belgium

[5] NASA Goddard Institute for Space Studies, New York, NY USA

[6] The Graduate Center of the City University of New york

[7] University of Boulder, Colorado, USA

Abstract

The surface energy balance and meltwater production of the Greenland ice sheet (GrIS) are modulated by snow and ice albedo through the amount of absorbed solar radiation. Here we show, using spaceborne multispectral data collected during the three decades from 1981 to 2012, that summertime surface albedo over the GrIS decreased at a statistically significant (99 %) rate of 0.02 decade^{-1} between 1996 and 2012. Over the same period, albedo modeled by the Modèle Atmosphérique Régionale (MAR) also shows a decrease, though at a lower rate (~ -0.01 decade^{-1}) than that obtained from spaceborne data. We suggest that the discrepancy between modeled and measured albedo trends can be explained by the absence in the model of processes associated with the presence of light-absorbing impurities. The negative trend in observed albedo is confined to the regions of the GrIS that undergo melting in summer, with the dry-snow zone showing no trend. The period 1981 – 1996 also showed no statistically significant trend

over the whole GrIS. Analysis of MAR outputs indicates that the observed albedo decrease is attributable to the combined effects of increased near-surface air temperatures, which enhanced melt and promoted growth in snow grain size and the expansion of bare ice areas, and by trends in light-absorbing impurities (LAI) on the snow and ice surfaces. Neither aerosol models nor in-situ and remote sensing observations indicate increasing trends in LAI in the atmosphere over Greenland. Similarly, an analysis of the number of fires and BC emissions from fires points to the absence of trends for such quatities. This suggests that the apparent increase of LAI in snow and ice might be related to the exposure of a 'dark band' of dirty ice and to increased consolidation of LAI at the surface with melt, not to increased aerosol deposition. Albedo projections through the end of the century under different warming scenarios consistently point to continued darkening, with albedo anomalies averaged over the whole ice sheet lower by 0.08 in 2100 than in 2000, driven solely by a warming climate. Future darkening is likely underestimated because of known underestimates in modelled melting (as seen in hindcasts) and because the model albedo scheme does not currently include the effects of LAI, which have a positive feedback on albedo decline through increased melting, grain growth and darkening.

1 Introduction

The summer season over the Greenland ice sheet (GrIS) during the past two decades has been characterized by increased surface melting (Nghiem et al., 2012; Tedesco et al., 2011, 2014) and net mass loss (Shepherd et al., 2012). Notably, the summer of 2012 set new records for surface melt extent (Nghiem et al., 2012) and duration (Tedesco et al., 2013), and a record of 570 ±100 Gt in total mass loss, doubling the average annual loss rate of 260 ±100 Gt for the period 2003–2012 (Tedesco et al., 2014).

Net solar radiation is the most significant driver of summer surface melt over the GrIS, (van den Broeke et al., 2011; Tedesco et al., 2011), and is determined by the combination of the amount of incoming solar radiation and surface albedo. Variations in snow albedo are driven principally by changes in snow grain size and by the presence of light-absorbing impurities (LAI , Warren and Wiscombe, 1982). Generally, snow albedo

is highest immediately following new snowfall. In the normal course of *destructive metamorphism* the snow grains become rounded, and large grains grow at the expense of small grains, so the average grain radius r increases with time (LaChapelle, 1969). Subsequently, warming and melt/freeze cycles catalyse grain growth, decreasing albedo mostly in the near-infrared (NIR) region (Warren 1982). The absorbed solar radiation associated with this albedo reduction promotes additional grain growth, further reducing albedo, potentially accelerating melting. The presence of LAI such as soot (black carbon, BC), dust, organic matter, algae and other biological material in snow or ice also reduces the albedo, mostly in the visible and ultraviolet regions (Warren 1982). Such impurities are deposited through dry and wet deposition, and their mixing ratios are enhanced through snow water loss in sublimation and melting (Conway et al., 1996; Flanner et al., 2007; Doherty et al., 2013). Besides grain growth and LAI, another cause of albedo reduction over the GrIS is the exposure of bare ice: once layers of snow or firn are removed through ablation, the exposure of the underlying bare ice will further reduce surface albedo, as does the presence of melt pools on the ice surface (e.g., Tedesco et al., 2011).

Most of the studies examining albedo over the whole GrIS have focused on data collected by the Moderate Resolution Imaging Spectroradiometer (MODIS) starting in 2000 (e.g., Box et al., 2012; Tedesco et al., 2013). At the same time, regional climate models (RCMs) have been employed to simulate the evolution and trends of surface quantities over the GrIS back to the 1960s using reanalysis data for forcing (e.g., Fettweis et al, 2012). Despite the increased complexity of models, and their inclusion of increasingly sophisticated physics parameterizations, RCMs still suffer from incomplete representation of processes that drive snow albedo changes, such as the spatial and temporal distribution of LAI, and from the absence of in-situ grain size measurement to validate modeled snow grain-size evolution. In this study, we first report the results from an analysis of summer albedo over the whole GrIS from satellite for the period 1980 – 2012, hence expanding the temporal coverage with respect to previous studies. Then, we combine the outputs of an RCM and in-situ observations with the satellite albedo estimates to identify those processes responsible for the observed albedo trends. The model, Modèle Atmosphérique Régionale (MAR), is used to simulate surface

temperature, grain size, exposed ice area, and surface albedo over Greenland at large spatial scales. MAR-simulated surface albedo is tested against surface albedo retrieved under the Global LAnd Surface Satellite (GLASS) project, and it is used to attribute trends in GLASS albedo. Lastly, we project the evolution of mean summer albedo over Greenland using the MAR model forced with the outputs of different Earth System Models (ESMs) under different CO_2 scenarios. Discussion and conclusions follow the presentation of the methods and results.

2 Methods and data

2.1 The MAR regional climate model and its albedo scheme

Simulations of surface energy balance quantities over the GrIS are performed using the Modèle Atmosphérique Régionale (MAR; e.g., Fettweis et al., 2005, 2013). MAR is a modular atmospheric model that uses the sigma-vertical coordinate to simulate airflow over complex terrain and the Soil Ice Snow Vegetation Atmosphere Transfer scheme (SISVAT, e.g., De Ridder and Gallée, 1998) as the surface model. MAR outputs have been assessed over Greenland in several studies (e.g., Tedesco et al., 2011; Fettweis et al., 2005; Vernon et al., 2013; Rae et al. 2012; Van Angelen et al., 2012), with recent work specifically focusing on assessing simulated albedo over Greenland (Alexander et al., 2014). A discussion of this evaluation is presented later in the manuscript. The snow model in MAR is the CROCUS model of Brun et al., (1992), which calculates albedo for snow and ice as a function of snow grain properties, which in turn are dependent on energy and mass fluxes within the snowpack. The model configuration used here has 25 terrain-following sigma layers between the Earth's surface and the 5-hPa-model top. The spatial configuration of the model uses the 25-km horizontal resolution computational domain over Greenland described in Fettweis et al. (2005). The lateral and lower boundary conditions are prescribed from meteorological fields modelled by the global European Centre for Medium-Range Weather Forecasts (ECMWF) Interim Reanalysis (ERA-Interim, http://www.ecmwf.int/en/research/climate-reanalysis/era-interim). Sea-surface temperature and sea-ice cover are also prescribed in the model using the same reanalysis data. The atmospheric model within MAR interacts with the CROCUS model, which provides the state of the snowpack and associated quantities (e.g., albedo, grain

size). No nudging or interactive nesting was used in any of the experiments.

The MAR albedo scheme is summarized below. Surface albedo is expressed as a function of the optical properties of snow, the presence of bare ice, whether snow is overlying ice (and whether the surface is waterlogged), and the presence of clouds. In the version used here (MARv 3.5.1), the broadband albedo (α_s, 0.3 – 2.8 μm) of snow is a weighted average (Eq. 1) of the albedo in three spectral bands, α_1, α_2 and α_3, which are functions of the optical diameter of snow grains (*d*, in meters), as modified from equations by Brun et al. (1992; e.g., Lefebre et al., 2003; Alexander et al., 2014):

$$\alpha_s = 0.58\alpha_1 + 0.32\alpha_2 + 0.10\alpha_3 \quad (1)$$

$$\alpha_1 = \max(0.94, 0.96 - 1.58\sqrt{d}), (0.3 - 0.8\ \mu m) \quad (2)$$

$$\alpha_2 = 0.95 - 15.4\sqrt{d}, (0.8 - 1.5\ \mu m) \quad (3)$$

$$\alpha_3 = 364 * \min(d, 0.0023) - 32.31\sqrt{d} + 0.88, (1.5 - 2.8\ \mu m) \quad (4)$$

The optical diameter *d* is, in turn, a function of snow grain properties and it evolves as described in Brun et al., (1992). In MAR, the albedo of snow is calculated by Eqs. 1-4, but it is not permitted to drop below 0.65.

For the transition from snow to ice, MAR makes the albedo an explicit function of density. On a polar ice sheet, densification of snow/firn/ice occurs in three stages, with a different physical process responsible for the densification in each stage (Herron and Langway, 1980; Arnaud et al., 2000). Newly-fallen snow can have density in the range 50-200 kg m^{-3}. After then, densification can occur due to wind processes, which break and round grains forming windslab of density typically around 300-400 kg m^{-3}. The remaining densification happens by *grain-boundary sliding*, attaining a maximum density of ~ 550 kg m^{-3} at the surface. Old melting snow at the surface in late summer typically has this density, but does not exceed it, because this is the maximum density that can be attained by grain-boundary sliding and corresponds to the density of random-packing of spheres (Benson, 1962, page 77). Further increases of density (the second stage) occur in *firn* under the weight of overlying snow, by *grain deformation* (pressure-sintering). In this case the density range is 550-830 kg m^{-3}. At a density of 830 kg m^{-3} the air becomes

closed off into bubbles and the material is called *ice*. In the third stage, the density of ice increases from 830 to 917 kg m^{-3} by shrinkage of air bubbles under pressure. Moving down the slope along the surface of the GrIS, at the transition between the accumulation area and the ablation area, the snow melts away, exposing firn. Continuing farther down, the firn melts away, exposing ice. The albedo of firn may be approximated as a function of its density, ρ, interpolating between the minimum albedo of snow and the maximum albedo of ice. In MAR these values of albedo are set to 0.65 and 0.55, respectively. We would then have for the density range of firn (550-830 kg m^{-3}):

$$\alpha_{firn} = 0.55 + (0.65-0.55)\ (830-\rho)/(830-550) \quad (5)$$

The MARv3.5.1 version used here maintains a minimum albedo of 0.65 for any density up to 830 kg m^{-3}, and specifies the gradual transition from snow albedo to ice albedo across the density range 830-920 kg m^{-3}. This means that the albedo of exposed firn is not allowed to drop below 0.65, with the result that the positive feedbacks of snow/firn/ice albedo will be muted in MAR. This aspect is being addressed in future versions of MAR (MAR v3.6) and a sensitivity analysis is being conducted to evaluate the impact of the changes on the albedo values when snow is transitioning from firn to ice. Such analysis is computationally expensive and preliminary outputs will be published once available.

In MAR, the albedo for bare ice is a function of the accumulated surface meltwater preceding runoff and specified minimum ($\alpha_{i,min}$) and maximum ($\alpha_{i,max}$) bare ice values:

$$\alpha_i = \alpha_{i,\min} + (\alpha_{i,\max} - \alpha_{i,\min}) e^{(-M_{SW(t)}/K)} \quad (6)$$

Here $\alpha_{i,min}$ and $\alpha_{i,max}$ are set, respectively, to 0.4 and 0.55, K is a scale factor set to 200 kg m^{-2}, and $M_{SW(t)}$ is the time-dependent accumulated excess surface meltwater before runoff (in kg m^{-2}).

When a snowpack with depth less than 10 cm is overlying a layer with a density exceeding 830 kg m^{-3} (i.e., ice), the albedo in MAR is a weighted, vertically-averaged

value of snow albedo (α_S) and ice albedo (α_I; e.g., if snow depth is 3 cm then albedo is obtained by multiplying the snow albedo by 0.3 and adding the ice albedo multiplied by 0.7).. When the snowpack depth exceeds 10 cm, the value is set to α_S. The presence of clouds can increase snow albedo because they absorb at the same NIR wavelengths where snow also absorbs, skewing the incident solar spectrum to wavelengths for which snow has higher albedo (Figure 5 of Grenfell et al., 1981; Figure 13 of Warren, 1982; Greuell and Konzelman, 1994), in which case the albedos of snow and ice are adjusted based on the cloud fraction modelled by MAR (Greuell and Konzelman, 1994).

2.2 The GLASS albedo product

The GLASS surface albedo product (http://glcf.umd.edu/data/abd/) is derived from a combination of data collected by the Advanced Very High Resolution Radiometer (AVHRR) and the MODerate resolution Imaging Spectroradiometer (MODIS, Liang et al., 2013). Shortwave broadband albedo (0.3 – 3 μm) is provided every 8 days at a spatial resolution of 0.05° (~56 km in latitude) for the period 1981 - 2012. GLASS albedo data with a resolution of 1 km is also available from 2000 to 2012 but it is not used here for consistency with the data available before 2000. There have been several efforts to make the AVHRR and MODIS albedo products consistent within the GLASS product, including the use of the same surface albedo spectra to train the regression and the use of a temporal filter and climatological background data to fill data gaps (Liang et al., 2013). Monthly averaged broadband albedos from GLASS-AVHRR and GLASS-MODIS were cross-compared over Greenland for those months when there was overlap (July 2000, 2003, and 2004), revealing consistency in GLASS retrieved albedo from the two sensors (He et al., 2013). More information on the GLASS data processing algorithm and product is available in Zhao et al. (2013) and Ying et al. (2014).

The GLASS product provides both black-sky albedo (i.e., albedo in the absence of a diffuse component of the incident radiation) and white-sky albedo (albedo in the absence of a direct component, with an isotropic diffuse component). The actual albedo is a value interpolated between these two according to the fraction of diffuse sunlight, which is a function of the aerosol optical depth (AOD) and cloud cover fraction. In the

absence of the full information needed to properly re-construct the actual albedo, here we use in our analysis the black-sky albedo, because we focus mostly on albedo retrieved under clear-sky conditions. Our analysis using the white-sky albedo (not shown here) is fully consistent with the results obtained using the black-sky albedo and reported in the following. A full description of the GLASS retrieval process and available products can be found in Liang et al. (2013) and references therein. An assessment of the GLASS product complementing existing studies is reported below.

Data collected by the MODIS TERRA and AQUA sensors are used in the GLASS albedo retrieval for the period 2000 – 2012 (2000 – 2012 for TERRA and 2002 – 2012 for AQUA, respectively). Wang et al. (2012) have shown that the MODIS TERRA sensor has been degrading at a pace that can be approximated by a second order polynomial, with the coefficients being spectrally dependent. Over Greenland, the impact of sensor degradation on albedo trends has been estimated at -0.0059 decade^{-1} (Stroeve et al., 2013). Polashenski et al. (2015) found a much greater impact on retrieved broadband albedo from TERRA sensor degradation (-0.03 decade^{-1}). However, Polashenski et al. (2015) use a daily product (MOD10A1) rather than a 16-day integrated product as in the case of GLASS (e.g., Ying et al., 2014), which does account for BRDF at high solar zenith angles. The performance of the MODIS daily product has been shown to deteriorate with latitude (e.g., Alexander et al., 2015). On the other hand, the use of the BRDF (as in the case of the GLASS product) improves the performance of the product at high latitudes (Alexander et al., 2015). This, together with the good agreement between the MCD43 albedo product and the surface station albedo data (Alexander et al., 2015) gives us confidence in the GLASS trends.

We complement previous assessments of the MODIS and GLASS albedo, evaluating the absolute accuracy of the GLASS retrievals by comparing monthly GLASS albedo to in-situ measurements of albedo collected at automatic weather stations of the Greenland climate network (GC-Net, Steffen and Box, 2001). GC-Net data are distributed at hourly temporal resolution and were temporally averaged to match the temporal window used in the GLASS product data. The root mean square error (RMSE), percentage RMSE (pRMSE), and the slope of a linear fit between GLASS and in-situ measured albedos for 12 stations are given in Table 1. The number of available years

used for the statistics is also reported for each station. We considered only stations for which at least 10 years were available for the analysis in at least one of the months. Our results are consistent with the findings reported by Alexander et al. (2014) and Stroeve et al., (2013, 2006) concerning the assessment of the MODIS albedo products over the GrIS. The mean value of the RMSE for all stations is 0.04-0.05 in all months, with individual station values as high as 0.15 for station JAR1 in August and as low as 0.01 for Summit and Saddle stations in June. The relatively large RMSE value for JAR1 (and other stations located within the ablation zone) is probably due to heterogeneity of albedo values within the pixel containing the location of the station and to the point-scale nature of the in-situ observations. At Summit, where spatial inhomogeneity on the surface is small, it is reasonable to assume that the effect of spatial scale and heterogeneity on the comparison is smaller.

3 Results

3.1 Albedo trends

The time series of the mean summer GLASS albedo values between 1981 and 2012 over Greenland can be separated into two distinct periods (Figure 1a): the period 1981 - 1996, when albedo shows no trend and a second period, 1996 – 2012, when a statistically significant trend (99 %) is detected. The year 1996 was identified as yielding the highest value of the coefficient of determination when fitting the albedo timeseries with two linear functions using a variable breaking point.

The GLASS albedo shows significant darkening ($p<0.01$) of the surface of the GrIS for the 1996 – 2012 period, with the summer (JJA) albedo declining at a rate of 0.02 ± 0.004 decade^{-1} (Figure 1a). About 25% of this decline might be attributed to sensor degradation, per the analysis of Stroeve et al. (2013). However, the TERRA sensor degradation is spectrally dependant and temporally non linear (Wang et al., 2012). This, together with the fact that the GLASS product uses a combination of both TERRA and AQUA data (which reduces the impact of the TERRA sensor degradation) indicates that impact of the sensor degradation on the observed decline is much smaller than 25 %. Over the same period, MAR-simulated summer near-surface temperature increased at a

rate of 0.74±0.5ºC decade^{-1} (Figure 1b, $p<0.05$), consistent with observed enhanced surface melting (e.g., Fettweis et al., 2013). MAR simulations also point to positive trends between 1996 and 2012 in summer surface grain radius (0.12±0.03 mm /decade^{-1}, $p<0.01$, Figure 1c) and the extent of those regions where bare ice is exposed during summer (380±190 km^2 decade^{-1}, $p<0.01$, Figure 1d). There is no statistically significant trend in GLASS summer albedo or MAR-simulated surface grain size and bare ice extent for the 1981-1996 period. Simulated summer snowfall (not plotted in the figure) does not show a statistically significant trend for the period 1996 – 2012 ($p<0.1$, -1702±790 mmWE /decade^{-1}). Notably, strong negative summer snowfall anomalies from 2010 to 2012 are simulated by MAR, down to -1.5 standard deviations below the 1981 – 2012 mean. We suggest that for 2010 - 2012, in addition to surface melting, reduced summer snowfall might have played a key role in the accelerated decline in summer albedo.

3.2 Drivers: surface grain size and bare ice

Inter-annual variability in the mean summer GLASS albedo is captured by the MAR albedo simulations (Figure 1a). For the period when the darkening has been identified, MAR albedo values explain ~ 90 % (de-trended) of the spaceborne-derived summer albedo interannual variability. A multi-linear regression analysis indicates that, over the same period, the interannual variability of summer values of surface grain size and bare ice extent simulated by MAR explain, respectively, 54 % (grain size) and 65 % (bare ice) of the inter-annual variability of GLASS albedo when considered separately. When linearly combined, grain size, bare ice extent and snowfall explain ~ 85 % of the GLASS inter-annual variability, with the influence of summer new snowfall alone explaining only 44 % of the GLASS summer albedo variability.

The spatial distribution of observed summer albedo trends from space shows that the largest trends (in magnitude) occur over those regions where surface temperature, grain size, and bare ice exposure have also changed the most (Figure 2). In particular, darkening observed from space is most pronounced at lower elevations in southwest Greenland, with trends as large as -0.20±0.07 decade^{-1} (Figure *2*a; note that the colour bar

only goes down to -0.06 decade^{-1} for graphical purposes), where trends in the number of days when simulated surface temperature exceeds 0ºC (Figure *2*b), grain size (Figure *2*c) and the number of summer days when bare ice is exposed (Figure *2*d) are the largest.

While MAR is able to capture a large component of the observed variability in albedo retrieved by GLASS, the simulated albedo trend is smaller in magnitude than that estimated using the GLASS product. The largest differences occur along the southwest margin of the ice sheet (Figure 3), where a "dark band" of outcropping layers of ice containing large concentrations of LAI is known to be present on the surface (Wientjes et al., 2011). In this region the number of days when surface temperature exceeds 0ºC has increased, with trends of up to more than 20 days decade^{-1} along the margins of the GrIS (Figure 1b). During this time-period GLASS albedo values are as low as 0.30, lower than that of bare ice (i.e., 0.45), consistent with in-situ measured values of dirty ice (Wientjes et al., 2010; Bøggild et al., 2010). Figure 4 shows the spatial distribution of MAR and GLASS mean JJA albedo for year 2010 over an area centred on the dark band in southwest Greenland, as well as the time series of GLASS albedo averaged over the same ice-covered area contained within the region identified by the black rectangle in Figure *4*a. The black line in Figure *4*c shows the GLASS spatially-averaged albedo within this region, with the top and the bottom margins of the grey area indicating, respectively, the maximum and minimum albedo values within that area. Note that we included only pixels that contained 100 % ice in all years (i.e. coloured areas in Figure *4*a and b) in the calculation shown in Figure *4*c, so trends are not driven by exposure of underlying land surface. Mean summer albedo from GLASS decreased over this area between 2005 and 2012 from ~ 0.6 to ~ 0.45 (vs. a decrease simulated by MAR of 0.075). Minimum summer albedo across all years averaged over the region is ~0.4, but dips close to ~0.3 in 2010, a value consistent with dirty bare ice, as shown in previous studies (Wientjes et al., 2010; Wientjes et al., 2011; Bøggild, et. al., 2010). We hypothesise that the discrepancy along this dark band between MAR- and GLASS albedo values is likely due to trends in the concentrations of LAI in the snow and ice in this region, which are not currently captured by the model.

3.3 Drivers: light-absorbing impurities on the surface of the GrIS

MAR simulations of albedo in different spectral bands (see Eqs. 1-4) point to comparable trends in the visible (0.3 – 0.8 μm; -0.009±0.005 decade^{-1}, $p<0.05$) and near-infrared (0.8 – 1.5 μm; -0.010±0.004 decade^{-1}, $p<0.05$) bands (Figure *5*a) and to a much smaller and not statistically significant trend in the shortwave infrared band (1.5 – 2.8 μm, -0.003±0.004 decade^{-1}, $p>0.1$). Because the GLASS product does not provide visible albedo (only broadband albedo), we extrapolated an estimate of the visible component of the GLASS albedo by subtracting the NIR and shortwave infrared albedo values computed with MAR from the GLASS broadband values, following the MAR albedo scheme (Eq. 1, Figure 5b). To evaluate the robustness of this approach, we compared anomalies (with respect to year 2000) in estimated GLASS visible albedo with those from the 16-day MODIS MCD43A3 product (Stroeve et al., 2013), which also has a visible albedo product (Figure *5*b). The MODIS albedo product we used is distributed by Boston University (https://lpdaac.usgs.gov/) and makes use of all atmospherically-corrected MODIS reflectance measurements over 16-day periods, to provide an averaged albedo every 8 days. A semi-empirical bidirectional reflectance distribution function (BRDF) model is used to compute bi-hemispherical reflectance from these reflectance measurements (Schaaf et al., 2002). The comparison between the GLASS- and MODIS-retrieved visible albedo anomalies is shown in Figure 5b, indicating that the two visible albedo anomalies are highly consistent, with a mean absolute error of 0.01 and a standard deviation of 0.005. There are differences in the estimated summer albedo trends from MCD43A3 and GLASS over the 2002 – 2012 period, with the former being -0.04±0.001 decade^{-1} and the latter -0.03±0.008 decade^{-1}. This difference could be due to the method we applied to estimate the visible component of the GLASS albedo, as well as other factors related to the data processing and algorithms used to extract albedo. Notably, however, the GLASS and MCD43 visible albedo trends are consistently about twice that estimated from the MAR model. The underestimated darkening by MAR relative to GLASS can be attributed to several factors, including the modeled spatial and temporal variability of the exposed bare ice area and the concentration of surface LAI on the ice surface, which is currently not included in the MAR albedo scheme. A lack of impurities in the MAR albedo scheme can affect simulated albedo trends in at least two ways: first,

the concentration of impurities over bare ice areas could be increasing, which would not be captured by MAR; second, the lack of impurities in the MAR albedo scheme causes bare ice areas to have an overestimated albedo. More frequent exposure of bare ice would lead to a decline in annual average albedo over time, but if the underlying bare ice is darker, such a trend would be larger. Thus, the difference in trends could result solely from an overestimation of the bare ice albedo by MAR. We are not able to discern the degree to which the difference is due to a) errors in the area and frequency of bare ice exposure from MAR; b) increasing concentration of impurities not captured by MAR, or c) overestimation of albedo of an unchanging impurity-covered bare ice surface. The study by Alexander et al. (2015) suggests that bare ice albedo is, indeed, overestimated in MAR. To test the impact of a fixed bare ice albedo on the simulated albedo trend, we performed a sensitivity experiment in which daily albedo for those pixels showing bare ice exposure is reduced by a fixed value of 0.1. The magnitude of the difference in trends between the original MAR simulation (with no change on the bare ice albedo) and the one with a modified albedo (Figure 6) is comparable to the difference between the MAR and GLASS trends (Figure 3a), suggests that this factor alone could explain the difference. To further investigate this aspect, we test the hypothesis of increased concentration of LAI on the snow and ice surface. The concentrations of LAI in surface snow and ice can increase either because of increased atmospheric deposition or because of post-depositional processes, including (a) loss of snow water to sublimation and melt, resulting in impurities accumulating at the surface as a lag-deposit (e.g., Doherty et al., 2013), and (b) the outcropping of 'dirty' underlying ice associated with snow/firn removal due to ablation. These processes are themselves driven by warming, and therefore constitute positive feedbacks.

Quantifying the contribution of surface LAI to GLASS summer albedo trends is a challenging task because of the relatively low impurity concentrations over most of the GrIS (Doherty et al., 2010; Bond et al., 2013), and because of known limitations related to remote sensing estimates of LAI from space (Warren, 2013). Moreover, quantifying the causes of potential increased impurity concentrations on the surface (atmospheric deposition vs. other factors) is also challenging, if not prohibitive, given the current state-of-the-art of spaceborne measurements (e.g. accuracy of the satellite products) and the

scarcity of in-situ data. Therefore, in the next section, we look for trends in forest fires and the emissions of BC from forest fires in the main source regions for aerosols over the GrIS and assess whether atmospheric aerosol concentrations over the GrIS have increased (as a proxy for whether the deposition of aerosol has increased).

3.4 Attribution: Aerosol contributions to LAI in GrIS

3.4.1 Trends in GrIS LAI

Ice core analyses of black carbon in the central regions of the GrIS have been used to study long-term variability and trends in pollution deposition (McConnell et al., 2007; Keegan et al., 2014). These records show that snow at these locations was significantly more polluted in the first half of the 20th century than presently. Both these records and in-situ measurements at Summit (Cachier and Pertuisot, 1994; Chylek et al., 1995; Hagler et al., 2007; Doherty et al, 2010) also indicate that in recent decades, the snow in central Greenland has been relatively clean, with concentrations smaller than 4 ng g^{-1} for BC. This amount of BC could lower snow albedo by only 0.002 for r=100 μm, or 0.005 for r=500 μm (Figure 5a of Dang et al., 2015). More recently, Polashenski et al. (2015) analysed BC and dust concentrations in 2012-2014 snowfall along a transect in northwest Greenland. They found similarly low concentrations of BC and concluded that albedo decreases in their study region are unlikely to be attributable to increases in BC or dust. Black carbon measurements from a high snowfall region of west central Greenland made on an ice core collected in 2003 show that black carbon concentrations varied significantly during the past 215 years, with an average annual concentration of 2.3 ng g^{-1} during the period 1952 – 2002, characterized by high year-to-year variability in summer and a gradual decline in winter BC concentrations through the end of the century (McConnell et al., 2007). Snow sampled in 1983 at Dye-3 had a median of 2 ng g^{-1} (Clarke and Noone, 1985). In 2008 and 2010, measurements 160 km away at Dye-2, using the same method, had medians of 4 ng g^{-1} in spring and 1 ng g^{-1} in summer (Table 9 of Doherty et al, 2010).

In the absence of in-situ measurements of impurity concentration trends over Greenland more broadly, or of trends in aerosol deposition rates (which are absent

entirely), we investigate trends in emissions from key sources of aerosols deposited to the GrIS and trends in Atmospheric Optical Depth (AOD) over GrIS.

3.4.2 Trends in fire count and BC emissions

Biomass burning in North America and Siberia is a significant source of combustion aerosol (BC and associated organics) to the GrIS (Hegg et al., 2009, 2010). Therefore, we investigated trends in the number of active fires in these two source regions, as well as BC emissions from fires in sub-regions within the northern hemisphere. For fire counts we used the MODIS monthly active fire products produced by the TERRA (MOD14CMH) and AQUA sensors (MYD14CMH) generated at 0.5° spatial resolution and distributed by the University of Maryland via anonymous ftp (http://www.fao.org/fileadmin/templates/gfims/docs/MODIS_Fire_Users_Guide_2.4.pdf, http://modis.gsfc.nasa.gov/data/dataprod/dataproducts.php?MOD_NUMBER=14). The results of our analysis are summarised in Figure 7, showing the standardised (subtracting the mean and dividing by the standard deviation of the 2002 – 2012 baseline period) cumulative number of fires (April through August) detected over North America (NA) and Eurasia (EU) by the MOD14CMH and MYD14CMH GCM climatology products between 2002 and 2012. The figure shows large inter-annual variability but no significant trend (at 90 % level) in the number of fires over the two areas between 2002 and 2012. The period between 2004 and 2011, when enhanced melting occurred over the GrIS, shows a negative trend (though also in this case not statistically significant).

In addition to number of fires we looked for trends specifically in BC emissions from fires in potential source regions for GrIS, using estimates from the Global Fire Emissions Database (GFED version 4.1, http://www.globalfiredata.org/). There is a great deal of inter-annual variability in annual BC emissions from fires in all regions (Figure 8), with no statistically significant increase during the 1997-2012 or 1997-2014 periods from either of the Boreal source regions or from Central Asia or Europe. BC emissions from fires in Temperate North America increased by, on average, 0.35×10^9 g yr^{-1} during 1997-2014 and by 0.52×10^9 g yr^{-1} 1997-2012 ($p<0.1$ in both cases), or an increase of 60% from 1997 to 2012. However, the total BC emissions from fires in this region constitute a small fraction of that from the Boreal regions. In addition, the only statistically

significant trend in regional BC emissions is a *decrease* in Central Asia (112.6x109 g yr-1; p-0.02), when GrIS albedo has declined most precipitously, is a *decrease* in BC emissions (-12.6x10^9 g yr^{-1}; p=0.02) in Central Asia. Xing et al. (2013, 2015) point out that direct anthropogenic emissions have also been decreasing across almost all of the mid- to high-latitude northern hemisphere.

3.4.3 Trends in AOD over Greenland

To investigate trends in AOD over GrIS we look at AOD as simulated by models and as measured at ground-based stations at several locations around the GrIS. AOD is a measure of the total extinction (omni-directional scattering plus absorption) of sunlight as it passes through the atmosphere, and is related to atmospheric aerosol abundance. Thus, it is a metric for the mass of aerosol available to be potentially deposited onto the GrIS surface. In the aerosol models, we are able to examine trends in total AOD as well as in aerosol components: BC, dust and organic matter. In addition, we examined trends in modelled deposition fluxes of these species to the GrIS.

For our analysis, we used model results from the Aerosol Comparisons between Observations and Models (AeroCom) project, an open international initiative aimed at understanding the global aerosol and its impact on climate (Samset et al., 2014; Myhre et al., 2013; Jiao et al., 2014; Tsigaridis et al., 2014). The project combines a large number of observations and outputs from fourteen global models to test, document and compare state-of-the-art modelling of the global aerosol. We specifically show standardised (i.e., subtracting the mean and then dividing by the standard deviation) deposition fluxes of BC, dust and organic aerosols (OA) from the GISS modelE contribution to the AeroCom phase II series of model runs (http://aerocom.met.no/aerocomhome.html). The runs used here took as input the decadal emission data from the Coupled Model Intercomparison Project Phase 5 (CMIP5). In this case, we report the outputs of the NASA GISS ModelE obtained from the AeroCom. In particular, Figures 9 and 10 show modelled deposition fluxes at the two locations of Kangerlussuaq (Figure 9, 67°00′31″N, 50°41′21″W) and Summit (Figure 10, 72º34′47″N, 38º27′33″W) for the months of June, July and August and aerosol components (BC, dust and organic matter). These locations were selected as representative of the ablation zone (Kangerlussuaq) and the dry-snow zone (Summit).

The analysis of the NASA GISS ModelE AeroCom outputs shows no statistically significant trend in the modelled fluxes for either location, consistent with the results recently reported by Polashenski et al. (2015) for the dry snow zone. Results of the analysis of fluxes over different areas point to similar conclusions. Similar results are obtained when considering the months of January, February and March, when aerosol concentration is expected to be higher. The results here presented complement other studies (e.g. Stone et al., 2014) indicating that, since the 1980s, atmospheric concentrations of BC measured at surface stations in the Arctic have decreased, with variations attributed to changes in both anthropogenic and natural aerosol and aerosol precursor emissions.

Mean summer values of AOD (550 nm) measured at three AERONET (http://aeronet.gsfc.nasa.gov) Greenland sites based in Thule (northwest Greenland; 77°28′00″N, 69°13′50″W), Ittoqqortoormiit (east-central Greenland; 70°29′07″N, 21°58′00″W), and Kangerlussuaq during the period 2007 – 2013 (with the starting year ranging between 2007 and 2009, depending on the site) are reported in Table 2, together with their standard deviations. None of the stations show statistically significant trends in AOD, consistent with the results of the analysis of the modelled deposition fluxes.

A recent study (Dumont et al., 2014) concluded that dust deposition has been increasing over much of the GrIS and that this is driving lowered albedo across the ice sheet. That conclusion was based on trends of an "impurity index", which is the ratio of the logarithm of albedo in the 545-565 nm MODIS band (where LAI affect albedo) to the logarithm of albedo in the 841-876 nm band (where they do not). In the MODIS product used in Dumont et al. (2014) study, albedo values rely on removal of the effects of aerosols in the atmosphere. In the Dumont et al. (2014) study this correction was made using simulations of atmospheric aerosols by the Monitoring Atmospheric Composition and Climate (MACC) model. Their resulting "impurity index" shows positive trends, and these are attributed in part (up to 30%) to increases in atmospheric aerosol not accounted for by the model, and the remainder to increases in snow LAI. The latter is consistent with our findings herein: that GrIS darkening is in part attributable to an increase in the impurity content of surface snow. However, Dumont et al. (2014) assume that this

increase in surface snow LAI is a result of enhanced deposition from the atmosphere. They do not account for the possibility that positive trends in impurity content may instead be a result of a warming-driven in-snow processes. Indeed, their own table shows variable AOD at AERONET stations in Greenland, but no trend over the period studied (2007 – 2012).

The results of the analysis discussed above reinforce our argument that the decline in the visible albedo over Greenland is probably not due to an increase in the rate of deposition of LAI from the atmosphere, but instead are due to the consolidation of LAI at the snow surface with warming-driven increases in melt and/or sublimation and with the increased exposure of underlying dirty ice.

4 Albedo projections through 2100

We estimated future projections of summer albedo over the GrIS using MAR forced with the outputs of three different Earth System Models (ESMs) from CMIP5 driven by two radiative forcing scenarios (Meinshausen et al., 2011) over the 120-year period 1980 – 2100. The first scenario corresponds to an increase in the atmospheric greenhouse gas concentration to a level of 850 ppm CO_2 equivalent (RCP45); the second scenario increases CO_2 equivalent to > 1370 ppm in 2100 (RCP85) (Moss et al., 2010; Meinshausen et al., 2011). The three ESMs used are the second generation of the Canadian Earth System Model (CanESM2), the Norwegian Community Earth System Model (NorESM1) and the Model for Interdisciplinary Research on Climate (MIROC5) of the University of Tokyo, Japan. More information is available in Tedesco and Fettweis (2012). The ESMs are used to generate MAR outputs for the historical period (1980 – 2005) and for future projections (2005 – 2100). The Canadian Earth System Model (CanESM2, e.g. Arora and Boer, 2010, Chylek et al., 2011) combines the fourth generation climate model (CanCM4) from the Canadian Center for Climate Modelling and Analysis with the terrestrial carbon cycle based on the Canadian Terrestrial Ecosystem Model (CTEM), which models the land-atmosphere carbon exchange. The NorESM1 model is built under the structure of the Community Earth System Model (CESM) of the National Center for Atmospheric Research (NCAR). The major difference from the standard CESM configuration concerns a modification to the treatment of

atmospheric chemistry, aerosols, and clouds (Seland et al., 2008) and the ocean component. Lastly, MIROC5 is a coupled general circulation model developed at the Center for Climate System Research (CCSR) of the University of Tokyo, composed of the CCSR/NIES (National Institute of Environmental Studies) atmospheric general circulation model (AGCM 5.5) and the CCSR Ocean Component Model, including a dynamic-thermodynamic sea-ice model (e.g., Watanabe et al., 2010, 2011). We refer to Tedesco and Fettweis (2012) for the evaluation of the outputs of MAR when forced with the outputs of the ESMs during the historical period (1980 – 2005). All simulations consistently point to darkening accelerating through the end of the century (Figure 11), with summer albedo anomalies (relative to year 2000) as large as -0.08 by the end of the century over the whole ice sheet, and even greater (-0.1) over the western portion of the ice sheet (Figure 12). The magnitude of the projected albedo anomalies by 2100, however, is probably underestimated by our simulations, because (a) the model tends to underestimate melting when forced with the ESMs (Fettweis et al., 2013), and therefore underestimates grain size growth, and (b) the model currently does not account for the presence of LAI in the snow or on the ice surface, nor for the positive feedback between LAI and snow/ice melt..

5 Discussion

Our results show a darkening of the GrIS 1996-2012, and indicate that this darkening is associated with increased surface snow grain size, an expansion in the area and persistence of bare ice, and by an increase in surface snow light-absorbing impurity (LAI) concentrations. We find no evidence for general increases in the deposition of LAI across the GrIS, so we associate the higher surface snow impurity concentrations predominantly with the appearance of underlying dirty ice and the consolidation of LAI in surface snow resulting from snow melt. Inter-annual variability in the JJA GLASS albedo is captured by the MAR albedo simulations, with the latter explaining ~ 90 % of the spaceborne-derived albedo interannual variations for the period 1996 - 2012. The strong correlation between MAR and GLASS albedo time series for this period suggests that MAR is capturing the processes driving most of the albedo inter-annual variability (grain size metamorphism and bare ice exposure) and that these processes have more influence than those associated with the spatial and temporal variability of surface

impurity concentrations at seasonal timescales (currently not included in the MAR albedo scheme).This is reinforced by the fact that the range of snow grain size found across the GrIS produces larger changes in albedo than does the range of LAI concentrations measured over the GrIS, at least in the cold-snow and percolation zones of the ice sheet. As pointed out by Tedesco et al. (2015), for pure snow, grain growth from new snow (with r = 100 μm) to old melting snow (r = 1000 μm) can reduce broadband albedo by ~ 10%. By comparison, adding 20 ng g^{-1} of BC, which has been found in the top layer of melting GrIS snow, reduces albedo by only 1-2%, consistently with the results reported by Polashenski et al. (2015).

Modeled (MAR) and retrieved (GLASS) albedo are compared, with the latter showing stronger declines in GrIS albedo, particularly over the ablation zone. Based on our analysis, we suggest that the difference between MAR and GLASS trends cannot be driven solely by the MODIS sensor degradation on the TERRA satellite (also used in the GLASS product), because the estimated impact of sensor degradation on the albedo trend is much smaller than the difference between the MAR and GLASS trends, and because the GLASS product is obtained by combining data from both TERRA and AQUA satellites, hence likely reducing the impact of the TERRA sensor degradation on the trends. This is especially true over the dark zone, where substiantial melting occurs and where the albedo decline is pronounced. As mentioned, a lack of impurities in the MAR albedo scheme can affect simulated albedo trends in at least two ways: first, the concentration of impurities over bare ice areas could be increasing or/and the lack of impurities in the MAR albedo scheme causes bare ice areas to have an overestimated albedo. Moreover, more frequent exposure of bare ice would lead to a decline in annual average albedo over time, with such a trend being larger in the case of the presence of impurity concentrations on the ice surface. Our sensitivity analysis of the simulated trends on the bare ice albedo value indicates that the difference between MAR and GLASS estimated trends is consistent with a relatively darker (e.g., containing LAI) bare ice. Since MAR does not account for the presence of surface LAI, and because the impact of LAI is mostly in the UV and visible portion of the spectrum, we suggest that another mechanism explaining the difference of -0.017 $decade^{-1}$ between the MAR and GLASS visible albedo trends is associated withy increasing mixing ratios of LAI in surface snow

and ice on some parts of the GrIS. As we pointed out, this could be due to a combination of increased exposure of dirty ice with ablation (Wientjes and Oerlemans, 2010; Bøggild et al., 2010), to enhanced melt consolidation with warming (e.g., Doherty et al., 2013), or to increased deposition of LAI from the atmosphere. The absence of in-situ, spatially distributed measurements to separate these processes means that we cannot quantify their relative contributions to the darkening in the visible region. Based on our analysis of trends in AOD over Greenland and the lack of a trend in forest-fire counts and BC in North America and Eurasia, we argue that increased deposition of LAI is not a large driver for the observed negative trends in Greenland surface albedo. An exception could be an increase in the deposition of locally-transported dust near the glacial margins, which would primarily affect the ablation zone. In particular, locally lofted dust may be playing a substantial role in the southwest GrIS ablation zone. However, we note that increased deposition is not needed in order to have an increase in the concentration of LAI at the GrIS surface. As noted above, indeed, temperatures and melt rates have been accelerating over the GrIS during the past decades (e.g., Tedesco et al., 2014). When snow melts, snow water is removed from the surface more efficiently than particulate impurities; the result is an increase in impurity concentrations in surface snow (e.g. Flanner et al., 2007; Doherty et al., 2013). Large particles, such as dust, in particular, will have poor mobility through the snowpack (Conway et al., 1996) so their concentration at the surface is expected to increase with snowmelt. This effect may be especially amplifying snow impurity content in the low-altitude ablation zone of the GrIS, where enhanced melting has been occurring (e.g., Tedesco et al., 2014). Further, the albedo reduction for a given concentration of an absorbing impurity in snow is greater in large-grained snow than in small-grained snow (Figure 7 of Warren and Wiscombe, 1980; Flanner et al., 2007), so climate warming itself will amplify the effect of LAI on surface albedo. Warming may also lead to increased sublimation, removing snow water but not particles from the snow surface, again increasing concentrations of LAI in surface snow.

Snow and ice warmed by increased temperatures and higher LAI concentrations also promotes darkening via so-called 'bio-albedo',, with biological growth on the surface depressing the albedo. Green, pink, purple, brown and black pigmented algae, indeed, occur in melting snow and ice. Microbes can bind to particulates, including BC, retaining

them at the surface in higher concentrations than in the parent snow and ice. The magnitude of this source of darkening is currently unquantified, but as the climate warms and melt seasons lengthen, biological habitats are expected to expand, with their contribution to darkening likely increasing (Benning et al., 2014).

Quantifying the impact of aerosols on Greenland darkening is also made difficult by the large disagreements among models in their predicted aerosol deposition rates over the GrIS. We examine the contrast between AOD trends from the MACC model used by Dumont et al., (2014) and the Goddard Chemistry Aerosol Radiation and Transport model (GOCART). The GOCART model simulates major tropospheric aerosol components, including sulphate, dust, BC, organic carbon (OC), and sea-salt aerosols using assimilated meteorological fields of the Goddard Earth Observing System Data Assimilation System (GEOS DAS), generated by the Goddard Global Modeling and Assimilation Office. Figure 13 compares results for AOD at 550 nm from MACC and GOCART for dust, organic matter and black carbon for the domain bounded by 75 to 80°N and 30 to 50° W (the same area considered by Dumont et al., 2014). The MACC model shows statistically significant trends for dust ($p<0.01$) and for total aerosols ($p<0.05$). All remaining trends are not statistically significant for both MACC and GOCART outputs (Figure 13).

Neither model represents the process of increased exposed silt/dust as Greenland glaciers receed; therefore, we would not expect them to capture trends in dust from this source. The inconsistency between the MACC and GOCART values and trends is puzzling, and indicates that the simulation of aerosol deposition rates over Greenland needs improvement.

6 Summary and conclusions

We studied the mean summer broadband albedo over the Greenland ice sheet between 1981 and 2012 as estimated from spaceborne measurements and found that summer albedo decreased at a rate of 0.02 decade^{-1} between 1996 and 2012. The analysis of the outputs of the MAR regional climate model indicates that the observed darkening is associated with increasing temperatures and enhanced melting occurring during the same period, which in turn promote increased surface snow grain size as well as the expansion and persistency of areas with exposed bare ice. The MAR model simulates

well the interannual variability in the retrieved GLASS albedo, but the albedo trend is larger in the GLASS albedo product than in MAR, indicating that processes not represented in the MAR physics account for some of the declining albedo. Specifically, we suggest that the absence of the effects of light-absorbing impurities in MAR could account for the difference. We also suggest that this hypothesis is supported by the trends observed along the ablation zone, where the diffrences between observed and modeled trends are more pronounced and the effect of the TERRA sensor degradation plays a relatively small role. On the other hand, over the dry snow zone, our hypothesis requires further testing, in view of the potentially higher impact of the sensor degradation on the observed albedo trend. The analysis of modelled fields and in-situ data indicated an absence of trends in aerosol optical depth over Greenland, as well as no significant trend in particulate light-absorbing emissions (e.g. BC) from fires in likely source regions. This is consistent with the absence of trends in surface aerosol concentrations measured around the Arctic. Consequently, we suggest that the increased surface concentrations of LAI associated with the darkening is not related to increased deposition of LAI, but rather to post-depositional processes, including increased loss of snow water to sublimation and melt and the outcropping of 'dirty' underlying ice associated with snow/firn removal due to ablation.

Future projections of GrIS albedo obtained from MAR forced under different warming scenarios point to continued darkening through the end of the century, with regions along the edges of the ice sheet subject to the largest decrease, driven solely by warming-driven changes in snow grain size, exposure of bare ice, and melt pool formation. We hypothesise that projected darkening trends would be even greater in view of the underestimated projected melting (and effect on albedo) and in view of the fact that the current version of the MAR model does not account for the presence of surface LAI and the associated positive direct and indirect impact on lowered albedo.

The drivers we identified to be responsible for the observed darkening are related to endogenous processes rather than exogenous ones and are strongly driven by melting. Because melting is projected to increase over the next decades, it is crucial to assess the state of the art of studying, quantifying and projecting these processes as they will

inevitably impact, and be impacted by, future scenarios. Intrinsic limitations of current observational tools and techniques, the scarcity of in-situ observations, and the albedo schemes currently used in existing models of surface energy balance and mass balance limit our ability to separate the contributions to darkening by the different processes, especially with regard to the cause and evolution of surface impurity concentrations. Moreover, as with all instruments, sensors undergo deterioration, and it can be difficult to separate an albedo trend from sensor drift. This is especially true in the dry-snow zone, where impurity concentrations are extremely low (only a few ppb in the case of BC). In this regard, a recent study by Polashenski et al. (2015) suggests that the decline and spectral shift in dry snow albedo over Greenland contains important contributions from uncorrected Terra sensor degradation when using the MODIS data collection C5. The new MODIS TERRA version (accounting for the sensor degradation) does not appear to show any trend (Polashenski, *Pers. Comm.),* hence supporting the hypothesis of the absence of trends of LAI deposition over the dry zone.

Remote sensing and in-situ observations should be complemented with models that simulate the surface energy balance to account for the evolution of the snowpack, in particular changes in surface grain size and exposure of bare ice. Simulations with regional climate models can provide such quantities, but they do not currently account for the transport and deposition of LAI to Greenland, the post-depositional evolution of impurities in the snowpack, and the synergism between surface LAI and grain growth (whereby a given impurity content causes more albedo reduction in coarse-grained snow than in fine-grained snow). In this regard, the current parameterisation for snow albedo in MAR is based on that of Brun et al. (1992), as part of an avalanche-forecasting model. As a consequence of the results of this study, we began evaluating an alternative albedo scheme using a parameterisation that can also account for the albedo reduction by absorptive impurities (e.g. Dang et al., 2015). Moreover, we are also considering using the firn/ice albedo parameterisation of Dadic et al (2013), based on measurements covering the range of densities from 400 to 900 kg m^{-3}.

Surface-based measurements are needed to test satellite-retrieved albedo and to quantify the drivers behind albedo changes in different areas of Greenland. To date, most surface-based observations have been made in the dry-snow zone or the percolation zone,

and they have generally focused on measuring the mixing ratios of BC (Hagler et al., 2007; McConnell et al., 2007, 2011; Polashenski et al., 2015) or of the spectral light absorption by all particulate components collectively (Doherty et al., 2010; Hegg et al., 2009, 2010). The regions of Greenland that are darkening the most rapidly are within the ablation zone. Here, there is no direct evidence that the rate of atmospheric deposition of LAI has been increasing. In view of the cumulative effect of snowmelt leaving impurities at the surface, the intra-seasonal variation of deposition may not be as important as the exposure of LAI by melting. Changes in the abundances of light-absorbing algae and other organic material with warmer temperatures may also be contributing to declining albedo, particularly for the ice, but this is an essentially un-studied source of darkening. Until measurements are made that quantify and distinguish the relative roles of each of these factors in the darkening of the GrIS, it is not possible to reduce the uncertainty in their contributions to the acceleration of surface melt. In addition to the need for targeted ground observations, it is necessary for the models that simulate and project the evolution of surface conditions over Greenland to start including the contribution of surface LAI, their processes, and their impact on albedo, as well as aerosol models that account for their deposition. Concurrently, spaceborne sensors or missions capable of separating the contributions from the different processes (with increased spatial, spectral and radiometric resolution) should be planned for remote sensing to become a more valuable tool in this regard.

Author contributions

MT conceived the study, carried out the scientific analysis and wrote the main body of the manuscript. SD co-wrote the manuscript and provided feedback on the analysis of the impact of surface LAI on the albedo decrease. PA provided MODIS visible data for the comparison with the GLASS-estimated visible albedo. JJ supported the reprojection and analysis of GLASS and MAR data. XF contributed with the analysis of MAR outputs. MT, SD, XF and JS edited the final version of the manuscript.

Acknowledgments

MT and PA were supported by NSF grants PLR1304807 and ANS 0909388, and NASA grant NNX1498G. The authors are grateful to Kostas Tsirigadis (NASA GISS) for

providing the outputs of GISS modelE of the AeroCom phase II project and to Marie Dumont, Eric Brun and Samuel Morin for the data used in Figure 13.

We thank Tao He at the University of Maryland, College Park, for the discussion on the GLASS product. The authors thank Stephen Warren for providing suggestions and guidance during the preparation of the manuscript, particularly for pointing out limitations and providing suggestions on the albedo parameterisations.

7 References

Alexander, P. M., Tedesco, M., Fettweis, X., van de Wal, R. S. W., Smeets, C. J. P. P. and van den Broeke, M. R.: Assessing spatio-temporal variability and trends (2000–2013) of modelled and measured Greenland ice sheet albedo, The Cryosphere, 8(4), 2293-2312, 2014.

Arnaud, L., J.M. Barnola, and P. Duval, Physical modeling of the densification of snow/firn and ice in the upper part of polar ice sheets. In *Physics of Ice Core Records* (T. Hondoh, Ed.), Hokkaido University Press, Sapporo, Japan, 285-305, 2000

Arora V. K. and Boer G. J., Uncertainties in the 20th century carbon budget associated with land use change *Glob. Change Biol.* **16**(12), 3327–3348, doi:10.1111/j.1365-2486.2010.02202.x, 2010

Benning, L. G., Anesio, A. M., Lutz, S. and Tranter, M.: Biological impact on Greenland's albedo, Nature Geosci, 7(10), 691–691, doi:10.1038/ngeo2260, 2014.

Benson, C.S., 1962: *Stratigraphic Studies in the Snow and Firn of the Greenland Ice Sheet.* Research Report 70, U.S. Army Snow, Ice, and Permafrost Research Establishment (SIPRE), 93 pp.

Bøggild, C.E., R.E. Brandt, K.J. Brown, and S.G. Warren (2010), The ablation zone in northeast Greenland: Ice types, albedos, and impurities. *J. Glaciol.,* **56**, 101-113.

Bond, T. C., S. J. Doherty, D. W. Fahey, P. M. Forster, T. Berntsen, B. J. DeAngelo, M. G. Flanner, S. Ghan, B. Kärcher, D. Koch, S. Kinne, Y. Kondo, P. K. Quinn, M. C. Sarofim, M. G. Schultz, M. Schulz, C. Venkataraman, H. Zhang, S. Zhang, N. Bellouin, S. K. Guttikunda, P. K. Hopke, M. Z. Jacobon, J. W. Kaiser, Z. Klimont, U. Lohmann, J. P. Schwarz, D. Shindell, T. Storelvmo, S. G. Warren and C. S. Zender, Bounding the Role of Black Carbon in Climate: A scientific assessment, J. Geophys. Res., 118(11), 5380-5552, doi:10.1002/jgrd.50171, 2013.

Box, J. E., Fettweis, X., Stroeve, J. C., Tedesco, M., Hall, D. K., and Steffen, K.: Greenland ice sheet albedo feedback: thermodynamics and atmospheric drivers, The Cryosphere, 6, 821-839, doi:10.5194/tc-6-821-2012, 2012.

Brun, E., David, P., Sudul, M. and Brunot, G.: A numerical model to simulate snow-cover stratigraphy for operational avalanche forecasting, Journal of Glaciology, 38(128), 13–22, 1992.

Cachier, H. and Pertuisot, M. H.: Particulate carbon in Arctic ice, Analusis Magazine, 22, 34–37, 1994

Ch´ylek, P., Johnson, B., Damiano, P. A., Taylor, K. C., and Clement, P.: Biomass burning record and black carbon in the GISP2 ice core, Geophys. Res. Lett., 22, 89–92, 1995. –

Chylek ,P., Li ,J., Dubey ,M. K., Wang ,M. and Lesins G., Observed and model simulated 20th century Arctic temperature variability: Canadian Earth System Model CanESM2 *Atmos. Chem. Phys. Discuss.* **11** 22893–22907, 2011

Clarke, A.D. and Noone, K.J.: Soot in the Arctic snowpack: A cause for perturbations in radiative transfer, Atmos. Environ., 19, 2045-2053, 1985.

Conway, H., A. Gades, and C. F. Raymond (1996), Albedo of dirty snow during conditions of melt, *Water Resour. Res.*, **32**(6), 1713–1718.

Dadic, R., P.C. Mullen, M. Schneebeli, R.E. Brandt, and S.G. Warren, 2013: Effects of bubbles, cracks, and volcanic tephra on the spectral albedo of bare ice near the Trans-Antarctic Mountains: implications for sea-glaciers on Snowball Earth. J. Geophys. Res. *(Earth Surfaces)*, 118, doi:10.1002/jgrf.20098.

Dang, C., R.E. Brandt, and S.G. Warren, 2015: Parameterizations for narrowband and broadband albedo of pure snow, and snow containing mineral dust and black carbon. *J. Geophys. Res.*, 120, doi:10.1002/2014JD022646.

De Ridder K., and Galle´ H. Land surface-induced regional climate change in Southern Israel,*Appl. Meteorol.*, 37, 1470-1485, 1998.

Doherty, S. J., Grenfell, T. C., Forsström, S., Hegg, D. L., Brandt, R. E. and Warren, S. G.: Observed vertical redistribution of black carbon and other insoluble light-absorbing particles in melting snow, Journal of Geophysical Research: Atmospheres, 118(11), 5553–5569, 2013.

Doherty, S. J., Warren, S. G., Grenfell, T. C., Clarke, A. D. and Brandt, R. E.: Light-absorbing impurities in Arctic snow, Atmos. Chem. Phys., 10(23), 11647–11680, 2010.

Dumont, M., Brun, E., Picard, G., Michou, M., Libois, Q., Petit, J.-R., Geyer, M., Morin, S. and Josse, B.: Contribution of light-absorbing impurities in snow to Greenland's darkening since 2009, Nature Geosci, 7(7), 509–512, 2014.

Fettweis, X., Franco, B., Tedesco, M., van Angelen, J. H., Lenaerts, J. T. M., van den Broeke, M. R. and Gallée, H.: Estimating the Greenland ice sheet surface mass balance contribution to future sea level rise using the regional atmospheric climate model MAR, The Cryosphere, 7(2), 469–489, 2013.

Fettweis, X., Gallée, H., Lefebre, F. and van Ypersele, J.-P.: Greenland surface mass balance simulated by a regional climate model and comparison with satellite-derived data in 1990–1991, Climate Dynamics, 24(6), 623–640, 2005.

Flanner, M. G., Zender, C. S., Randerson, J. T., and Rasch, P. J.: Present-day climate forcing and response from black carbon in snow, J. Geophys. Res., 112, D11202, doi:10.1029/2006JD008003, 2007.

Grenfell, T.C., D.K. Perovich, and J.A. Ogren, 1981: Spectral albedos of an alpine snowpack. *Cold Reg. Sci. Technol., 4,* 121-127.

Greuell, W. and Konzelman, T.: Numerical modelling of the energy balance and the englacial temperature of the Greenland Ice Sheet, Calculations for the ETH-Camp location (West Greenland, 1155 m a.s.l.), Global and Planetary Change, 9, 91–114, 1994.

Hagler, G. S. W., Bergin, M. H., Smith, E. A., and Dibb, J. E.: A summer time series of particulate carbon in the air and snow at Summit, Greenland, J. Geophys. Res., 112, D21309, doi:10.1029/2007JD008993, 2007.

He, T., Liang, S., Yu, Y., Wang, D., Gao, F. and Liu, Q.: Greenland surface albedo changes in July 1981–2012 from satellite observations, Environ. Res. Lett., 8(4), 044043, 2013.

Hegg, D. A., Warren, S. G., Grenfell, T. C., Doherty, S. J., Larson, T. V. and Clarke, A. D.: Source Attribution of Black Carbon in Arctic Snow, Environmental Science & Technology, 43(11), 4016–4021, 2009.

Hegg, D.A., S.G. Warren, T.C. Grenfell, S.J. Doherty, and A.D. Clarke, 2010: Sources of light-absorbing aerosol in Arctic snow and their seasonal variation. *Atmos. Chem. Phys.*, **10**, 10923-10938 .

Herron, M.M., and C.C. Langway, Jr., 1980: Firn densification: An empirical model. *J. Glaciol., 25,* 373-385.

Ichoku, C. and Ellison, L.: Global top-down smoke-aerosol emissions estimation using satellite fire radiative power measurements, Atmos. Chem. Phys., 14(13), 6643–6667, 2014.

Keegan, K. M., M. R. Albert, J. R. McConnell and I. Baker, climate change and forest fires synergistically drive widespread met events of the Greenland Ice Sheet, PNAS, 111, 7964-7967,doi: 10.1073/pnas.1405397111.

LaChapelle, E.R.: Field Guide to Snow Crystals, University of Washington Press, Seattle, 1969.

Jiao, C., et al.: An AeroCom assessment of black carbon in Arctic snow and sea ice, Atmos. Chem. Phys., 14(5), 2399–2417, 2014.

Lefebre, F., Gallée, H, and van Ypersele, J.-P.: Modeling of snow and ice melt at ETH Camp (West Greenland): a study of surface albedo,., 108, 4231, doi:10.1029/2001JD001160, 2003

Liang, S., et al.: A long-term Global LAnd Surface Satellite (GLASS) data-set for environmental studies, International Journal of Digital Earth, 6(sup1), 5–33, 2013.

Loeb, N.: In-flight calibration of NOAA AVHRR visible and near-IR bands over Greenland and Antarctica, International Journal of Remote Sensing, 18, 477–490, 1997.

Masonis, S. *J.* and Warren, S. G.: Gain of the AVHRR visible channel as tracked using bidirectional reflectance of Antarctic and Greenland snow, International Journal of Remote Sensing, 22, 1495–1520, 2001.

McConnell, J. R., R. Edwards, G. L. Kok, M. G. Flanner, C. S. Zender, E. S. Saltzman, J. R. Banta, D. R. Pasteris, M. M. Carter, and J. D. W. Kahl, 20th-century industrial black carbon emissions altered Arctic climate forcing, Science, 317(5843), 1381–1384, doi:10.1126/science.1144856, 2007.

McConnell, J. R., Edwards, R., Kok, G. L., Flanner, M. G., Zender, C. S. Saltzman, E. S., Banta, J. R., Pasteris, D. R., Carter, M. M., and Kahl, J. D. W.: 20th century industrial black carbon emissions altered Arctic climate forcing, Science, 317, 1381–1384, doi:10.1126/science.1144856, 2007.Meinshausen, et al..: The RCP greenhouse gas concentrations and their extensions from 1765 to 2300, Climatic Change, 109(1-2), 213–241, 2011.

Moss, R. H., et al.: The next generation of scenarios for climate change research and assessment, Nature, 463(7282), 747–756, 2010.

Myhre, et al.: Radiative forcing of the direct aerosol effect from AeroCom Phase II simulations, Atmos. Chem. Phys., 13(4), 1853–1877, 2013.

Nghiem, S. V., Hall, D. K., Mote, T. L., Tedesco, M., Albert, M. R., Keegan, K., Shuman, C. A., DiGirolamo, N. E. and Neumann, G.: The extreme melt across the Greenland ice sheet in 2012, Geophysical Research Letters, 39(20), L20502, 2012.

Polashenski, C. M., J. E. Dibb, M. G. Flanner, J. Y. Chen, Z. R. Courville, A. M. Lai, J. J. Schauer, M. M. Shafer, and M. Bergin: Neither dust nor black carbon causing apparent albedo decline in Greenland's dry snow zone: Implications for MODIS C5 surface reflectance, Geophys. Res. Lett., 42, 9319–9327, doi:10.1002/2015GL065912, 2015.

Rae, J. G. L., Aðalgeirsdóttir, G., Edwards, T. L., Fettweis, X., Gregory, J. M., Hewitt, H. T., Lowe, J. A., Lucas-Picher, P., Mottram, R. H., Payne, A. J., Ridley, J. K., Shannon, S. R., van de Berg, W. J., van de Wal, R. S. W. and van den Broeke, M. R.: Greenland ice sheet surface mass balance: evaluating simulations and making projections with regional climate models, The Cryosphere, 6(6), 1275–1294, 2012.

Rignot, E., Velicogna, I., van den Broeke, M. R., Monaghan, A. and Lenaerts, J. T. M.: Acceleration of the contribution of the Greenland and Antarctic ice sheets to sea level rise, Geophysical Research Letters, 38(5), L05503, 2011.

Samset, B. H., Myhre, G., Herber, A., Kondo, Y., Li, S. M., Moteki, N., Koike, M., Oshima, N., Schwarz, J. P., Balkanski, Y., Bauer, S. E., Bellouin, N., Berntsen, T. K., Bian, H., Chin, M., Diehl, T., Easter, R. C., Ghan, S. J., Iversen, T., Kirkevåg, A., Lamarque, J. F., Lin, G., Liu, X., Penner, J. E., Schulz, M., Seland, Ø., Skeie, R. B., Stier, P., Takemura, T., Tsigaridis, K. and Zhang, K.: Modeled black carbon radiative forcing and atmospheric lifetime in AeroCom Phase II constrained by aircraft observations, Atmospheric Chemistry and Physics Discussions, 14(14), 20083–20115, 2014.

Schaaf, C. B., Gao, F., Strahler, A. H., Lucht, W., Li, X., Tsang, T., Strugnell, N. C., Zhang, X., Jin, Y., Muller, J. P., Lewis, P., Barnsley, M., Hobson, P., Disney, M., Roberts, G., Dunderdale, M., Doll, C., d'Entremont, R. P., Hu, B., Liang, S., Privette, J. L. and Roy, D.: First operational BRDF, albedo nadir reflectance products from MODIS, Remote Sensing of Environment, 115, 1296–1300, 2002.

Seland, O., T. Iversen, A. Kirkevag and T. Storelvmo, Aerosol-climate interactions in the CAM-Oslo atmospheric GCM and investigation of associated basic shortcomings *Tellus A* **60** p 459–491. doi: 10.1111/j.1600-0870.2008.00318.x, 2008

Shepherd, A., et al.: A Reconciled Estimate of Ice-Sheet Mass Balance, Science, 338(6111), 1183–1189, 2012.

Steffen, K. and Box, J. E.: Surface climatology of the Greenland ice sheet: Greenland Climate Network 1995-1999, Journal of Geophysical Research, 106(D24), 33951–33964, 2001.

Stohl, A., et al.: Pan-Arctic enhancements of light absorbing aerosol concentrations due to North American boreal forest fires during summer 2004, J. Geophys. Res., 111(D22), D22214, 2006.

Stone, R. S., Sharma, S., Herber, A., Eleftheriadis, K. and Nelson, D. W.: A characterization of Arctic aerosols on the basis of aerosol optical depth and black carbon measurements, Elementa: Science of the Anthropocene, 2, 000027, 2014.

Stroeve, J., Box, J. E., Gao, F., Liang, S., Nolin, A. and Schaaf, C.: Accuracy assessment of the MODIS 16-day albedo product for snow: comparisons with Greenland in situ measurements, Remote Sensing of Environment, 94(1), 46–60, 2005.

Stroeve, J., Box, J. E., Wang, Z., Schaaf, C. and Barrett, A.: Re-evaluation of MODIS MCD43 Greenland albedo accuracy and trends, Remote Sensing of Environment, 138, 199–214, 2013.

Tedesco, M. and Fettweis, X.: 21st century projections of surface mass balance changes for major drainage systems of the Greenland ice sheet, Environ. Res. Lett., 7(4), 045405, 2012.

Tedesco, M., Fettweis, X., Broeke, M. R. V. D., Wal, R. S. W. V. de, Smeets, C. J. P. P., Berg, W. J. V. de, Serreze, M. C. and Box, J. E.: The role of albedo and accumulation in the 2010 melting record in Greenland, Environ. Res. Lett., 6(1), 014005, 2011.

Tedesco, M., Fettweis, X., Mote, T., Wahr, J., Alexander, P., Box, J. E. and Wouters, B.: Evidence and analysis of 2012 Greenland records from spaceborne observations, a regional climate model and reanalysis data, The Cryosphere, 7(2), 615–630, 2013.

Tedesco, M., S. Doherty, S. Warren, J. Stroeve, P. Alexander, X. Fettweis, and M. Tranter, 2015: What darkens the Greenland ice sheet? *EOS*, in press.

Tedesco,M., J. E. Box, J.Cappelen, X. Fettweis, T. Mote, A. K. Rennermalm, R. S. W. van de Wal and J. Wahr, 2014: Greenland Ice Sheet in [*2013 NOAA Arctic Report Card*]

Tsigaridis, K., et al.: The AeroCom evaluation and intercomparison of organic aerosol in global models, Atmospheric Chemistry and Physics Discussions, 14(5), 6027–6161, 2014.

van Angelen, J. H., Lenaerts, J. T. M., Lhermitte, S., Fettweis, X., Kuipers Munneke, P., van den Broeke, M. R., van Meijgaard, E. and Smeets, C. J. P. P.: Sensitivity of Greenland Ice Sheet surface mass balance to surface albedo parameterization: a study with a regional climate model, The Cryosphere, 6(5), 1175–1186, 2012.

van den Broeke, M. R., C. J. P. P. Smeets, and R. S. W. van de Wal, The seasonal cycle and interannual variability of surface energy balance and melt in the ablation zone of the west Greenland ice sheet, Cryosphere, 5, 377-390, doi:10.5194/tc-5-377-2011.

Vernon, C. L., Bamber, J. L., Box, J. E., van den Broeke, M. R., Fettweis, X., Hanna, E. and Huybrechts, P.: Surface mass balance model intercomparison for the Greenland ice sheet, The Cryosphere, 7(2), 599–614, 2013.

Wang, D., Morton, D., Masek, J., Wu, A., Nagol, J., Xiong, X., Levy, R., Vermote, E. and Wolfe, R.: Impact of sensor degradation on the MODIS NDVI time series, Remote Sensing of Environment, 119, 55–61, 2012.

Warren, S. G.: Optical properties of snow, Reviews of Geophysics and Space Physics, 20(1), 67–89, 1982.

Warren, S. G.: Can black carbon in snow be detected by remote sensing? Journal of Geophysical Research: Atmospheres, 118(2), 779–786, 2013.

Warren, S.G., and W.J. Wiscombe, 1980: A model for the spectral albedo of snow, II: Snow containing atmospheric aerosols. *J. Atmos. Sci.*, **37**, 2734-2745.

Watanabe et al, Improved Climate Simulation by MIROC5: Mean States, Variability, and Climate Sensitivity. *J. Climate*, **23**, 6312–6335, 2010

Watanabe S, Hajima T, Sudo K, Nagashima T, Takemura T, Okajima H, Nozawa T, Kawase H, Abe M, Yokohata T, Ise T, Sato H, Kato E, Takata K, Emori S and Kawamiya M 2011 MIROC-ESM: model description and basic results of CMIP5-20c3m experiments, *Geosci. Model Dev. Discuss.*, **4**, 1063-1128, doi:10.5194/gmdd-4-1063-2011

Wientjes, I. G. M. and Oerlemans, J.: An explanation for the dark region in the western melt zone of the Greenland ice sheet, The Cryosphere, 4(3), 261–268, 2010.

Wientjes, I. G. M., van de Wal, R. S. W., Reichart, G. J., Sluijs, A. and Oerlemans, J.: Dust from the dark region in the western ablation zone of the Greenland ice sheet, The Cryosphere, 5, 589–601, 2011.

Xing, J., Mathur, R., Pleim, J., Hogrefe, C., Gan, C. M., Wong, D. C., Wei, C., Gilliam, R. and Pouliot, G.: Observations and modeling of air quality trends over 1990–2010 across the Northern Hemisphere: China, the United States and Europe, Atmos. Chem. Phys., 15(5), 2723–2747, 2015.

Xing, J., Pleim, J., Mathur, R., Pouliot, G., Hogrefe, C., Gan, C. M. and Wei, C.: Historical gaseous and primary aerosol emissions in the United States from 1990 to 2010, Atmos. Chem. Phys., 13(15), 7531–7549, 2013.

Ying, Q., Qiang, L., Shunlin, L., Lizhao, W. Nanfeng, L. and Suhong L. : Direct-Estimation Algorithm for Mapping Daily Land-Surface Broadband Albedo From MODIS Data, *Geoscience and Remote Sensing, IEEE Transactions on* , vol.52, no.2, pp.907-919, 2014, doi: 10.1109/TGRS.2013.2245670

Zhao, X.; Liang, S.; Liu, S.; Yuan, W.; Xiao, Z.; Liu, Q.; Cheng, J.; Zhang, X.; Tang, H.; Zhang, X.; Liu, Q.; Zhou, G.; Xu, S.; Yu, K. The Global Land Surface Satellite (GLASS) Remote Sensing Data Processing System and Products. *Remote Sens.*, *5*, 2436-2450, 2013.

FIGURES

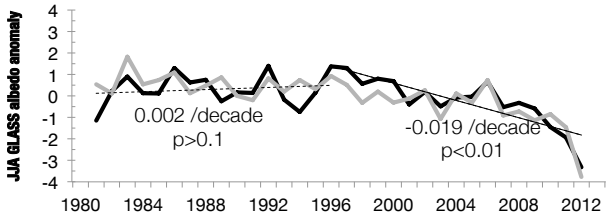

(a)

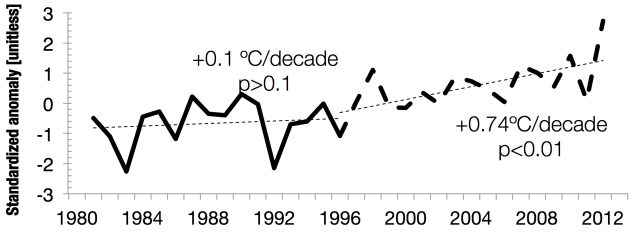

(b)

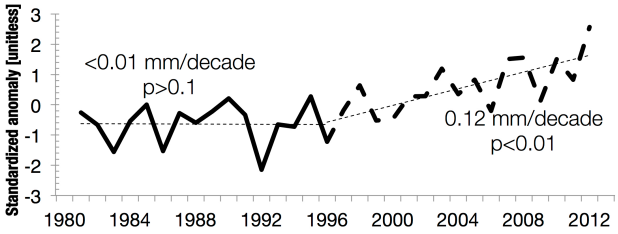

(c)

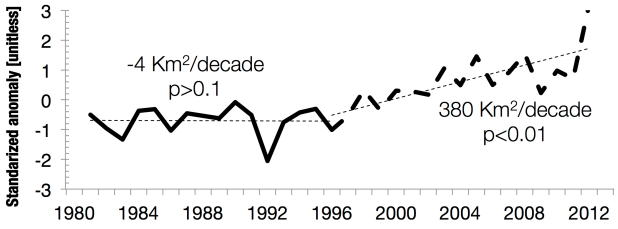

(d)

Figure 1 Mean summer standardized values plotted as time series for (a) albedo from GLASS (black) and MAR (grey), together with MAR-simulated values of (b) surface air temperature, (c) surface grain size (effective radius of optically "equivalent" sphere) and (d) bare ice exposed area. Trends for the periods 1981 – 1996 and 1996 – 2012 are reported in each plot. Trends in (a) refer to the GLASS albedo. The baseline 1981 – 2012 period is used to compute standardized anomalies, obtained by subtracting the mean and then dividing by the standard deviation of the values in the time series. All trends are computed from JJA averaged values over ice-covered areas only, not tundra.

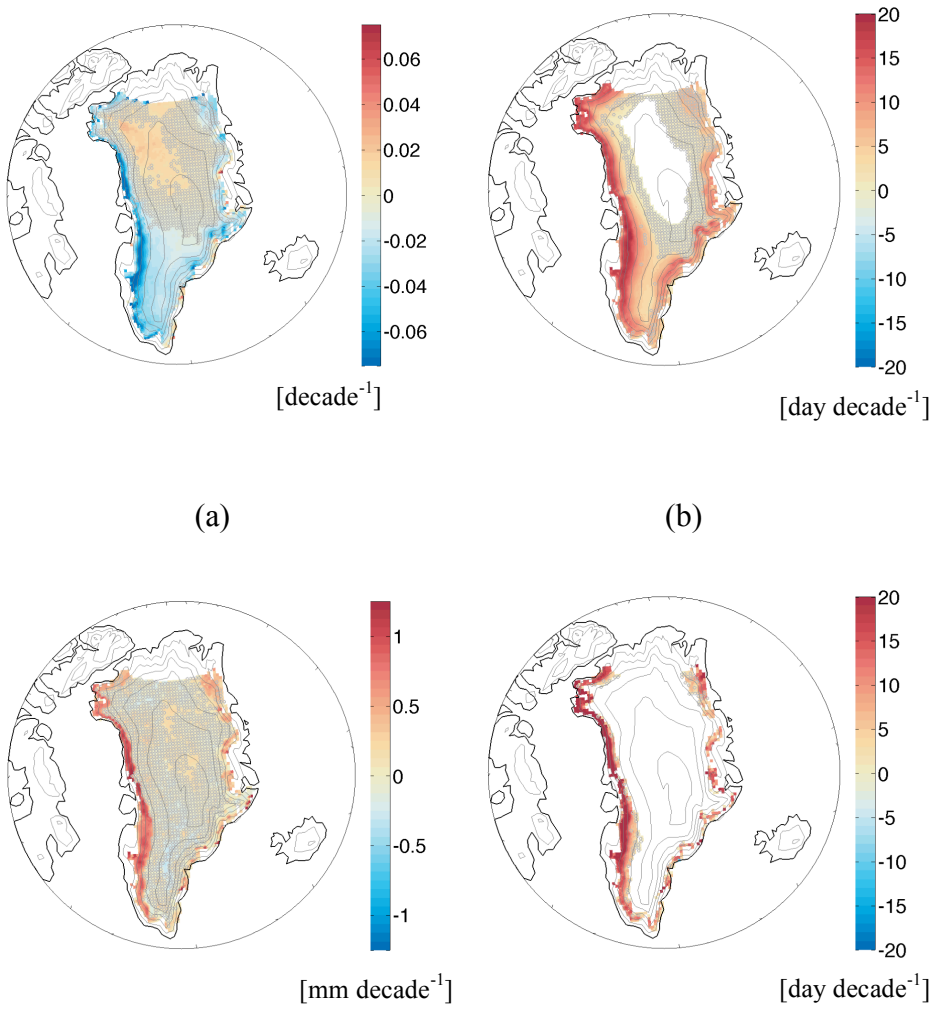

Figure 2 Maps of JJA trends (per decade) from 1996 to 2012, when darkening began to occur, for a) spaceborne estimated GLASS albedo, b) number of days when MAR-simulated surface air temperature exceeded 0ºC, c) MAR-simulated surface grain size and d) number of days when bare ice is exposed as simulated by MAR. Regions where trends are not significant at a 95 % level are shown as grey-hatched areas. White regions over the north end of the ice sheet indicate areas or were not viewed by the satellite.

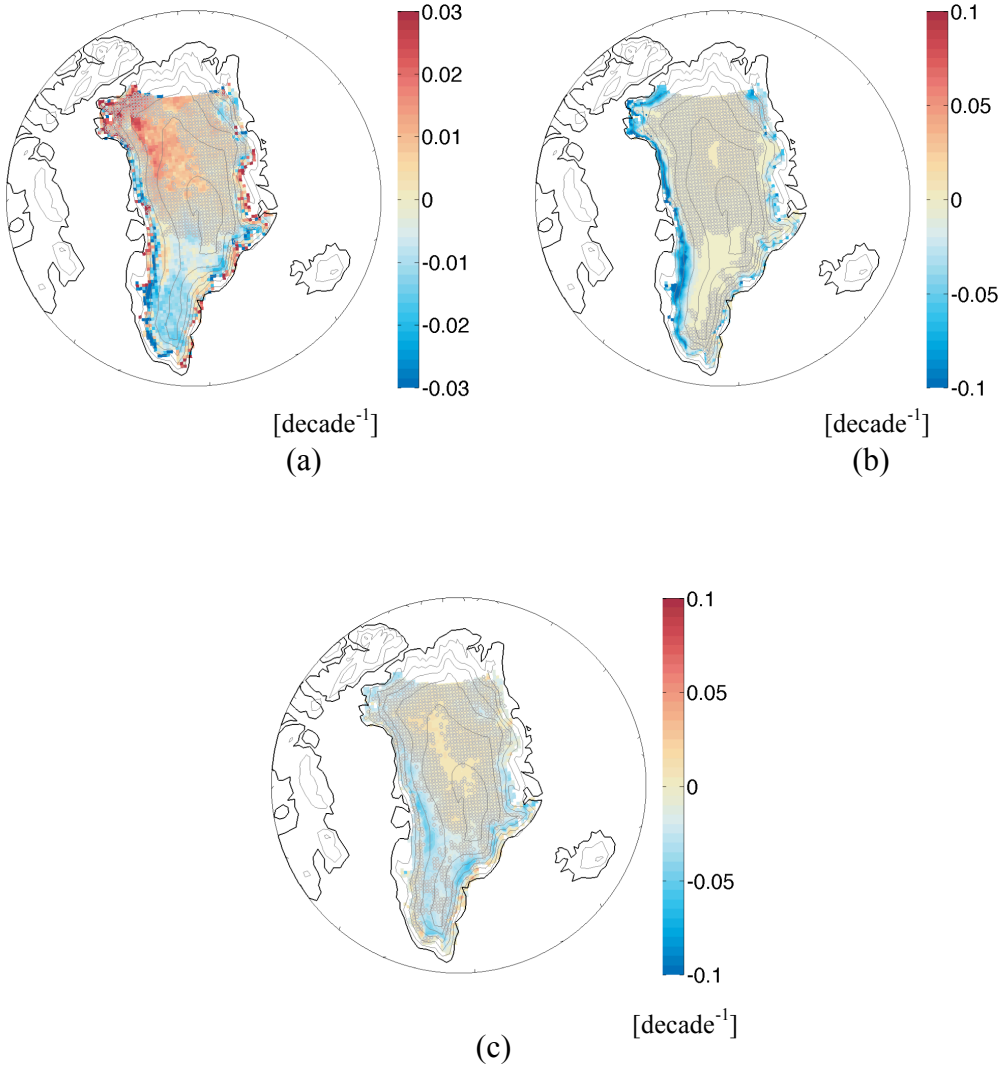

Figure 3 Differences between spaceborne measured and model-simulated albedo trends in different spectral regions. a) Difference between the GLASS and MAR trends (albedo change per decade), with positive values indicating those regions where MAR trend is smaller in magnitude than GLASS. Maps of JJA mean albedo trends (1996 – 2012) simulated by MAR for b) visible and c) near-infrared wavelengths.

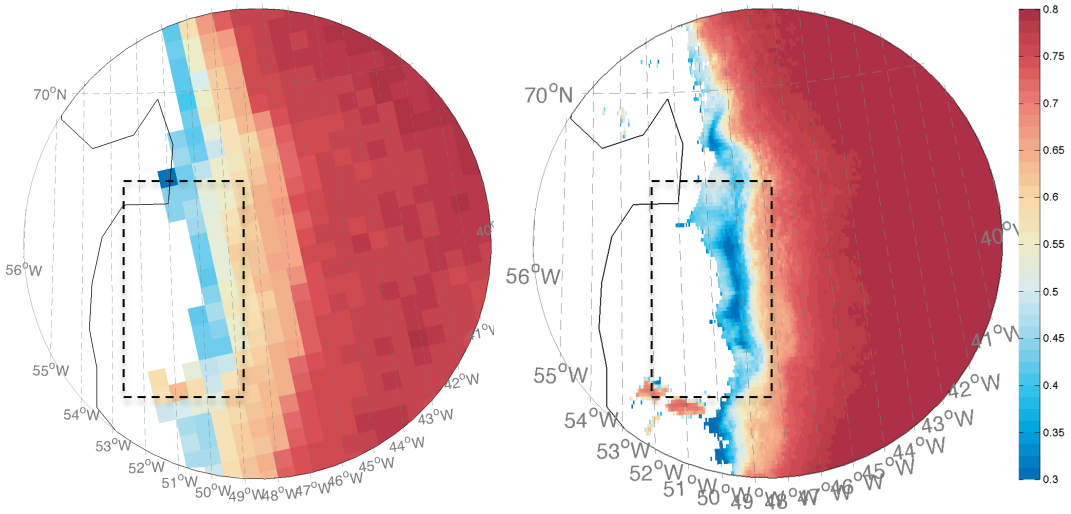

(a) (b)

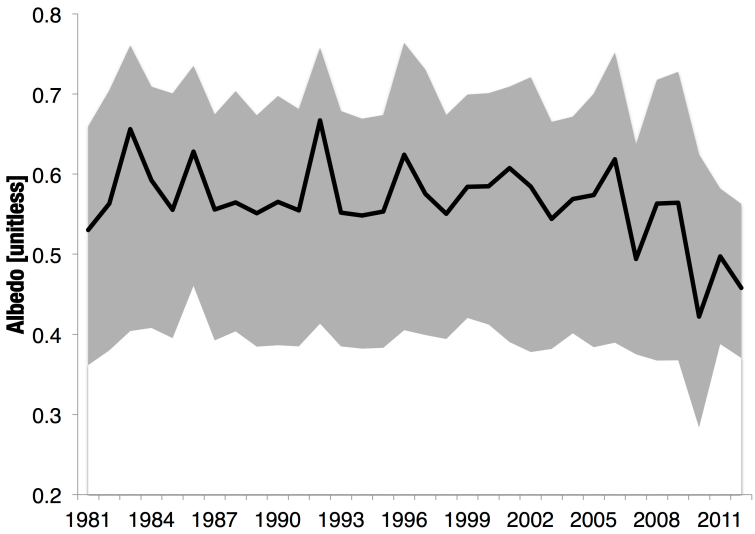

(c)

Figure 4 a) MAR and b) GLASS mean JJA albedo for year 2010 over an area including the dark band together with c) time series of mean JJA albedo for the ice-covered areas in the black rectangle. The black line in c) shows the GLASS spatially averaged albedo, where the top and the bottom of the grey area indicate, respectively, the maximum and minimum albedo within the black box in b).

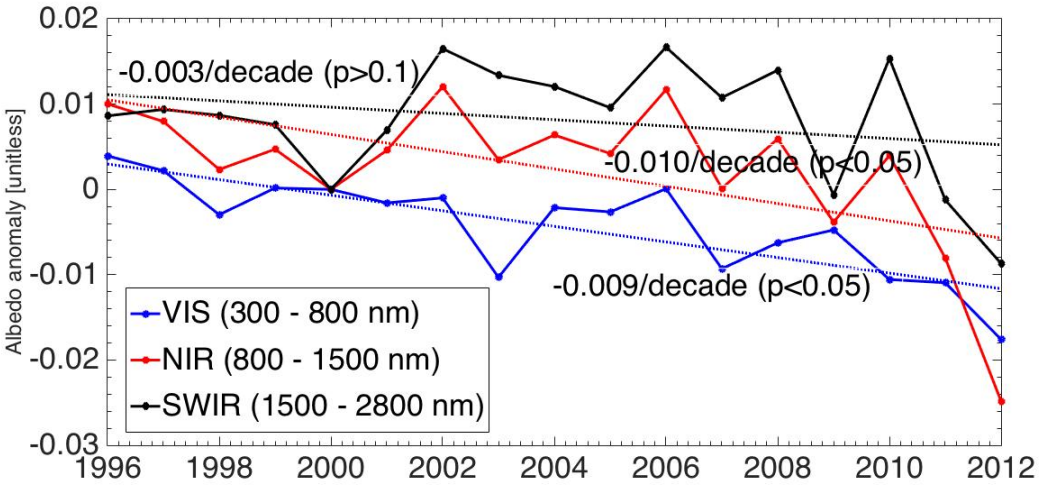

(a)

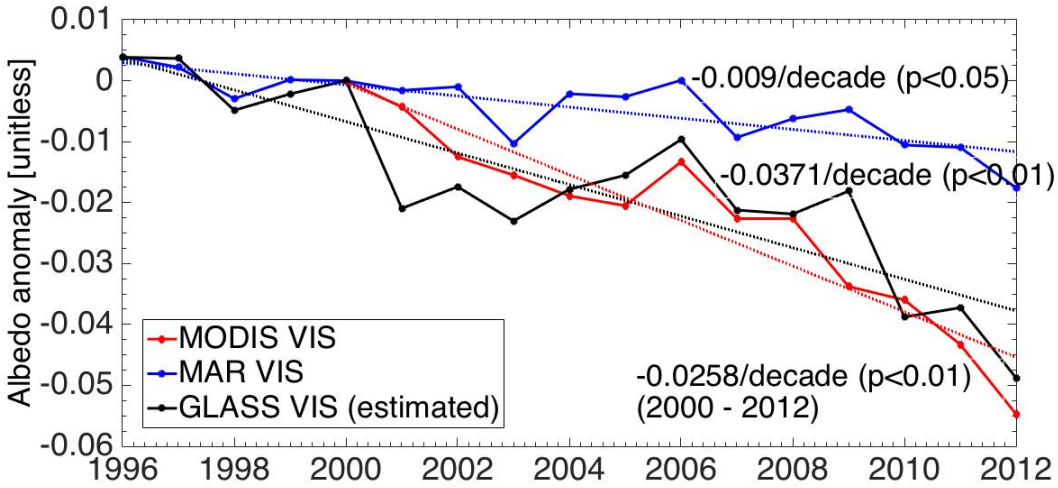

(b)

Figure 5 Time series of modelled and measured mean summer (JJA) albedo anomalies (with respect to year 2000) in different spectral bands. a) Visible, near-infrared and shortwave-infrared albedo values simulated by MAR; b) as in a) but for the visible albedo only from MAR, MODIS (obtained from the product MCD43) and GLASS. Note that the vertical axis scale in (b) is different from that in (a).

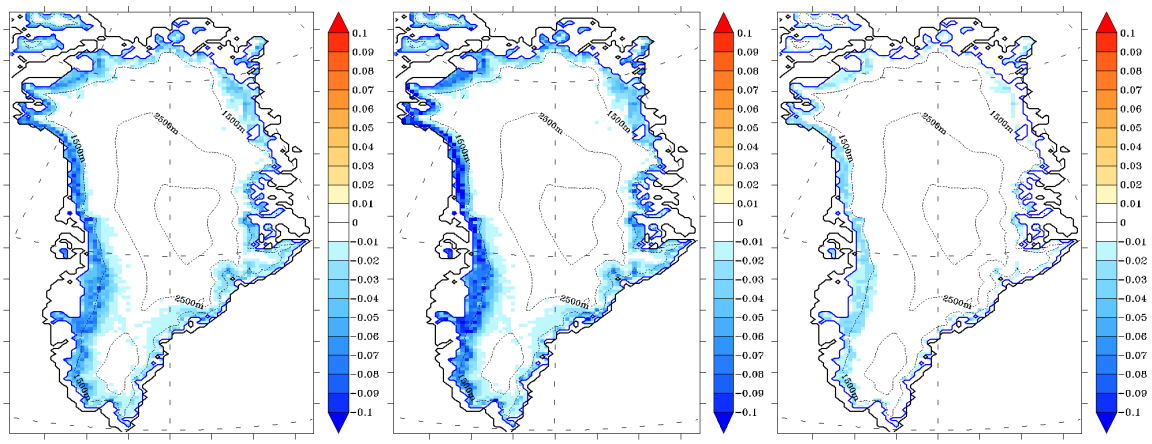

(a) *(b)* *(c)*

Figure 6 Maps of MAR-simulated albedo trends between 1996 and 2012 using a) the original MAR albedo scheme and b) the perturbated MAR outputs in which daily albedo is artificially decreased by 0.1 from the MAR-computed value for those regions where bare ice is exposed. c) Difference between the trends obtained with MAR original albedo scheme and the perturbated solution.

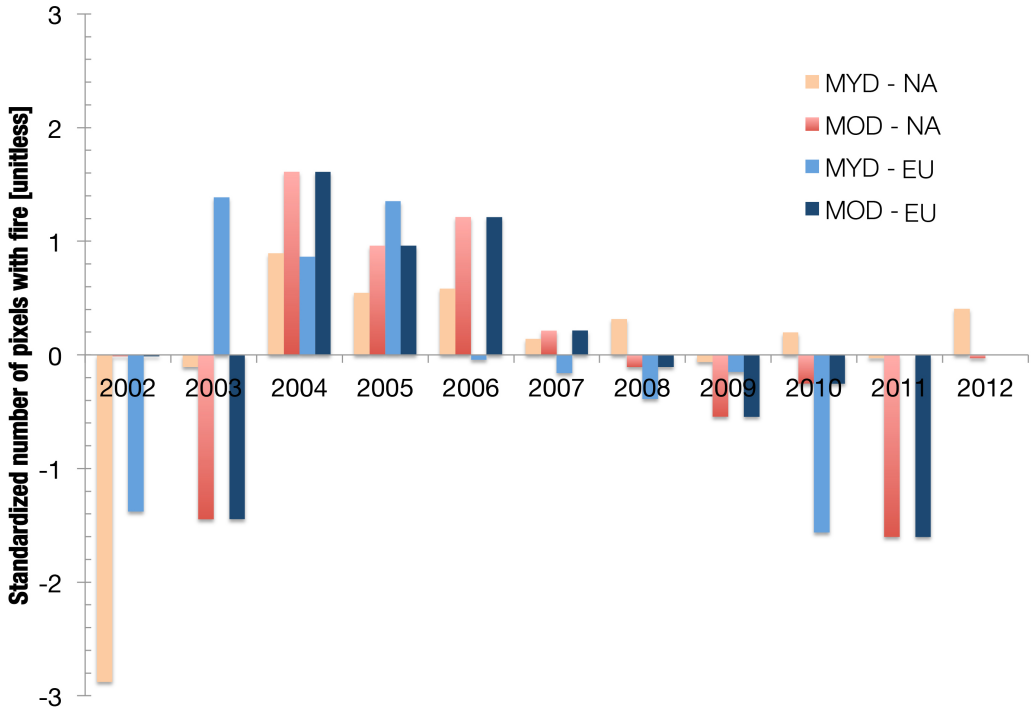

Figure 7 Standardised cumulative number of fires (April through August) detected over North America (NA) and Eurasia (EU) by the MOD14CMH and MYD14CMH GCM climatology products between 2002 and 2012.

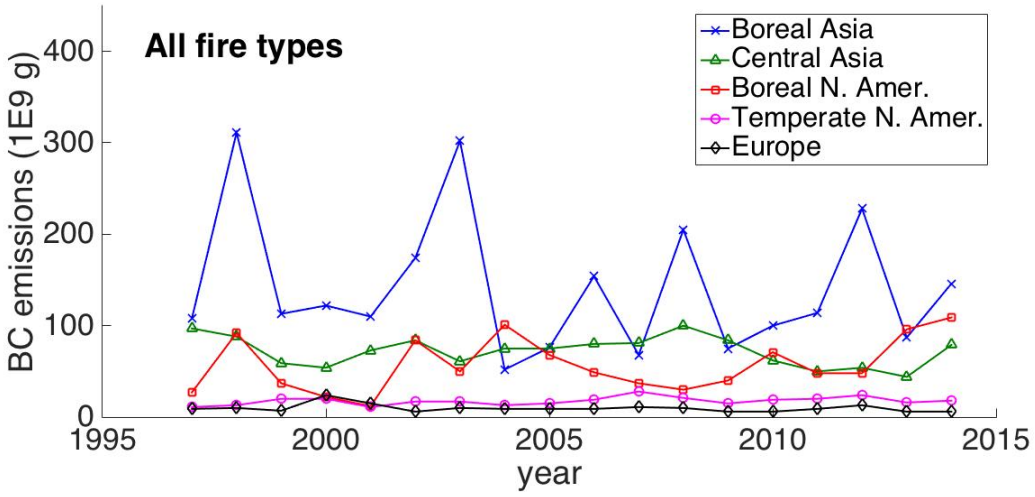

(a)

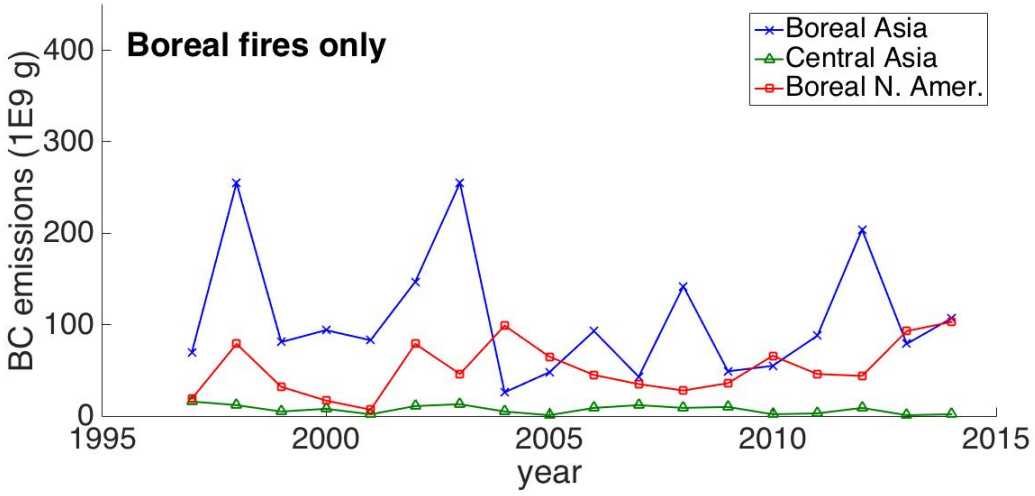

(b)

Figure 8 BC emissions [g] from fires in potential source regions for GrIS for a) all fire types and b) boreal fires only using estimates from the Global Fire Emissions Database (GFED version 4.1, http://www.globalfiredata.org/) between 1997 and 2014.

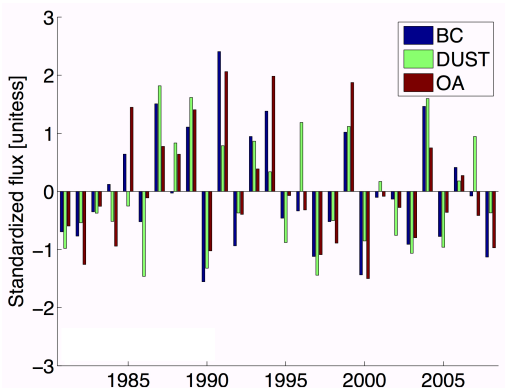

(a)

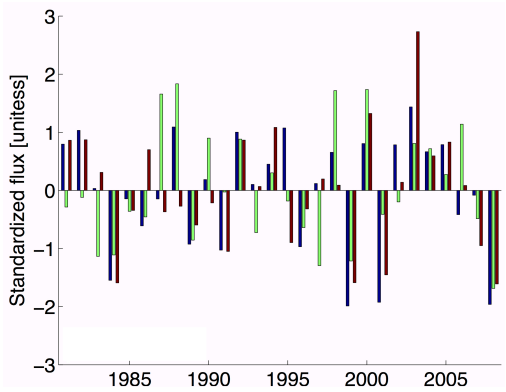

(b)

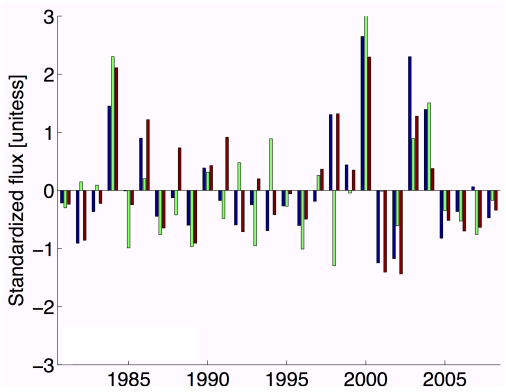

(c)

Figure 9 NASA GISS ModelE standardized deposition fluxes for BC, dust and organic aerosol at Kangerlussuaq for a) June, b) July and c) August (1981 – 2008) from the AEROCOM simulations.

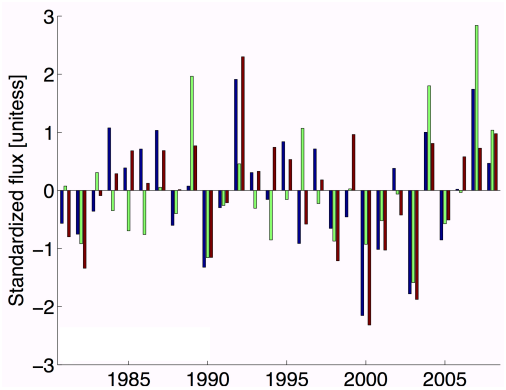

(a)

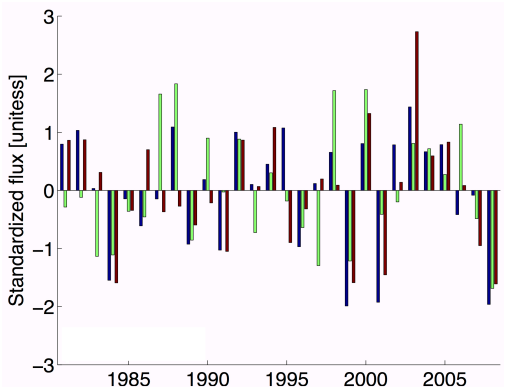

(b)

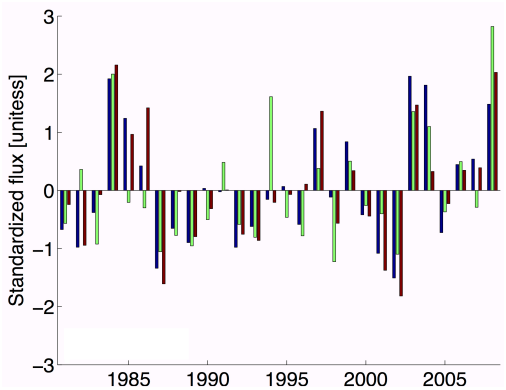

(c)

Figure 10 Same as Figure 9 but for Summit station.

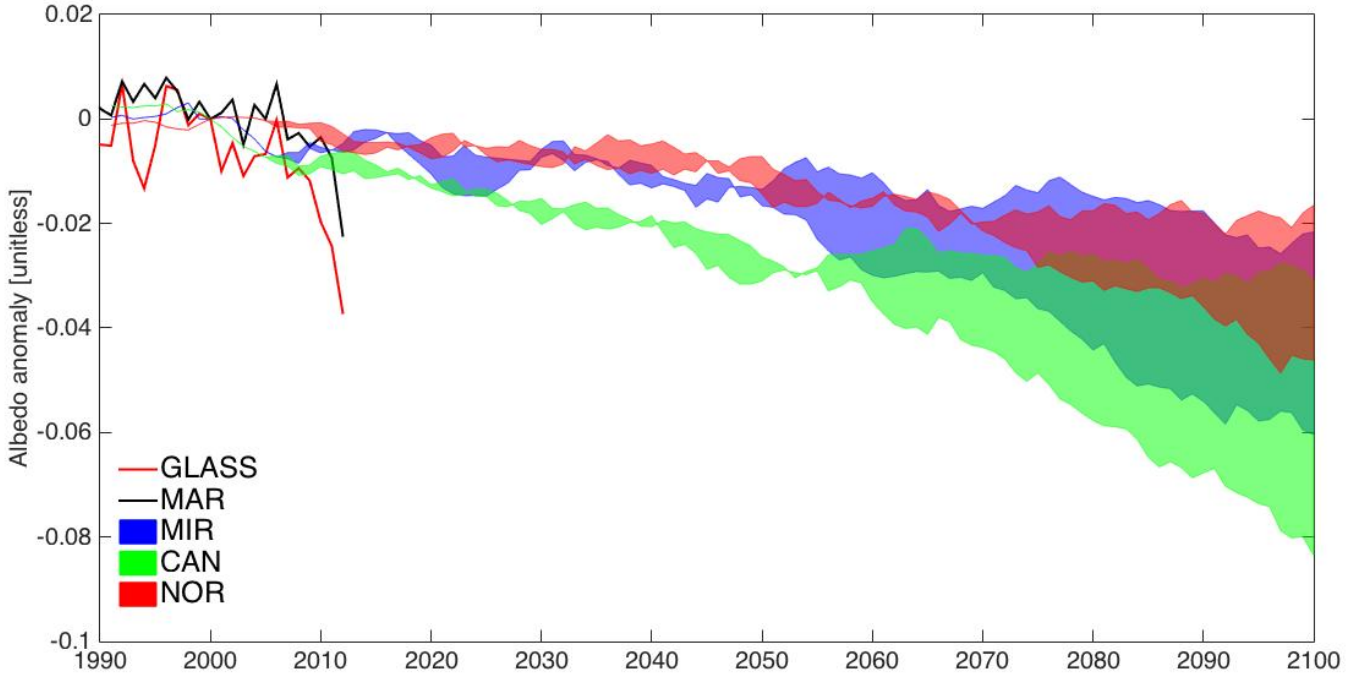

Figure 11 Projections of broadband albedo anomaly (with respect to year 2000) averaged over the whole GrIS for 1990-2012 from MAR simulations and GLASS retrievals (black and red lines, respectively), and as projected by 2100. Future projections are simulated with MAR forced at its boundaries with the outputs of three ESMs under two warming scenarios, with the first scenario (RCP45) corresponding to an increase in the atmospheric greenhouse gas concentration to a level of 850 ppm CO_2 equivalent by 2100 and the second (RCP85) to > 1370 pm CO_2 equivalent. The top and the bottom of the coloured area plots represent the results concerning the RCP45 (top) and RCP85 (bottom) scenarios. Semi-transparent colours are used to allow view of the overlapping data. Dark green corresponds to the case where MIROC5 and CANESM2 results overlap and brown to the case when the results from the three ESMs overlap.

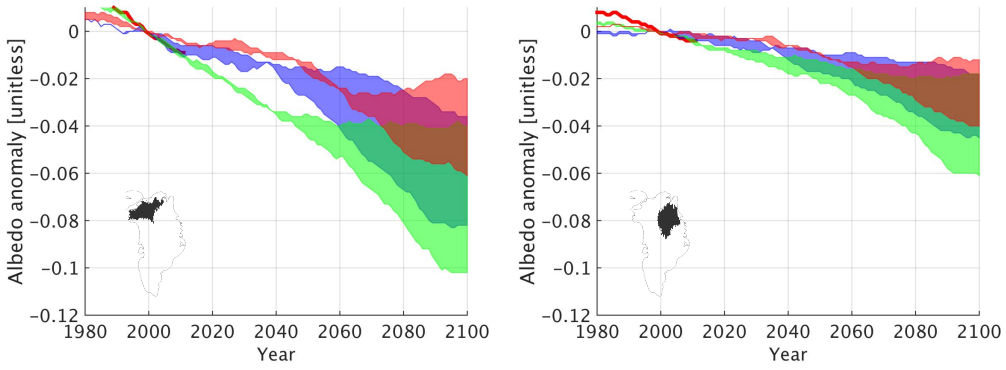

(a) (b)

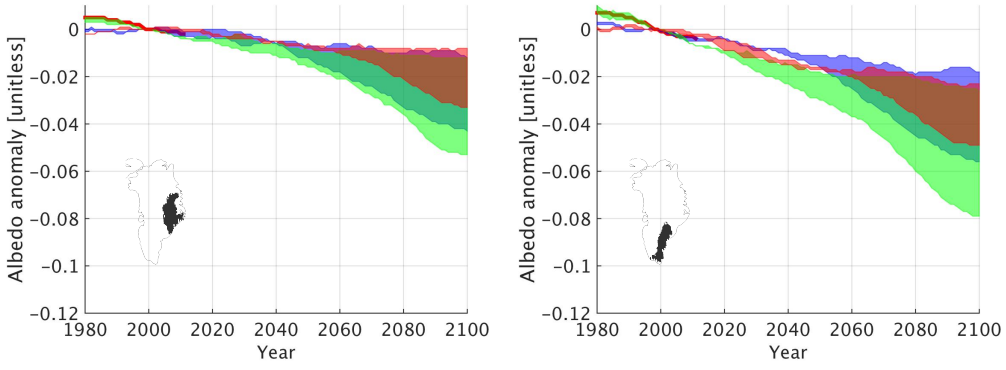

(c) (d)

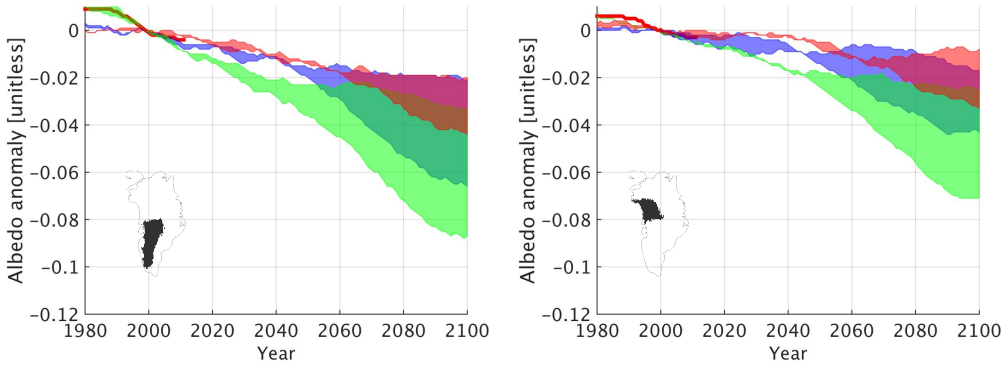

(e) (f)

Figure 12 Same as Figure 11 but for different drainage regions of the GrIS, indicated by the small maps in each panel. Color scheme for the shaded regions is the same as Figure 10. The top and the bottom of each area plots represent the results concerning the RCP45 (bottom) and RCP85 (top) scenarios. Red lines represent the GLASS albedo averaged over the corresponding drainage region.

	June				July				August				JJA			
Station	rmse	Rmsep [%]	slope	# of years	rmse	rmsep	slope	# of years	rmse	rmsep	slope	# of years	rmse	rmsep	slope	# of years
Swiss	0.12	19.60	-0.22	11	0.02	3.86	1.12	9	0.04	6.92	1.00	8	0.02	2.73	1.06	7
CP	0.07	8.72	0.12	12	0.06	7.40	0.14	14	0.06	7.21	0.11	13	0.07	8.20	-0.02	11
Humboldt	0.08	10.38	-0.16	8	0.07	9.31	0.35	9	0.08	9.98	0.39	10	0.07	9.42	0.27	8
Summit	0.01	1.45	0.85	15	0.02	2.25	-0.25	16	0.01	1.71	-0.68	16	0.01	1.22	0.12	15
TunuN	0.05	6.72	-0.66	15	0.06	7.89	0.79	15	0.07	8.84	0.69	15	0.06	7.53	0.37	15
Dye-2	0.02	2.58	0.57	14	0.02	2.15	0.75	14	0.01	1.73	0.68	15	0.01	1.54	0.82	12
Jar1	0.06	8.45	0.68	13	0.10	23.80	0.68	15	0.15	43.55	0.22	14	0.07	14.24	0.66	12
Saddle	0.01	1.28	0.94	14	0.02	1.95	0.61	14	0.01	1.75	0.46	14	0.01	1.31	0.71	14
NASAE	0.03	4.23	0.46	14	0.05	5.97	0.14	14	0.04	5.11	0.24	14	0.04	4.97	0.24	14
NASA SE	0.02	2.76	0.59	13	0.02	2.32	0.67	13	0.02	2.14	0.36	14	0.02	2.23	0.56	13
JAR2	0.06	12.27	0.20	11	0.05	10.00	-0.10	12	0.06	11.96	-0.06	11	0.04	8.51	0.16	10
Mean	0.048	7.13			0.0455	6.99			0.05	9.2			0.038	5.62		

Table *1* Comparison between GLASS retrieved albedo and GC-NET in -situ albedo measurements, for monthly- and seasonally-averaged albedos at twelve surface stations on the Greenland ice sheet.

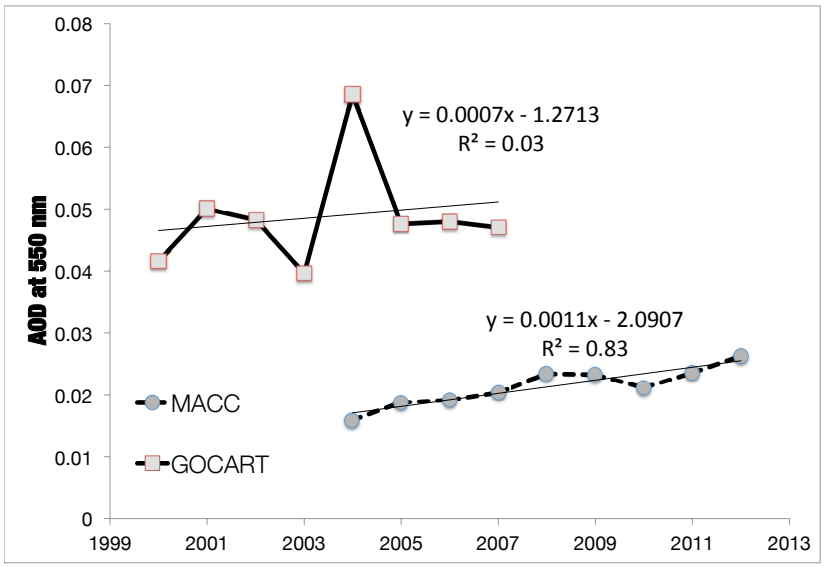
0.08
0.07
0.06
0.05
0.04
0.03
0.02
0.01
0
AOD at 550 nm
y = 0.0007x - 1.2713
R² = 0.03
y = 0.0011x - 2.0907
R² = 0.83
MACC
GOCART
1999
2001
2003
2005
2007
2009
2011
2013

(a)

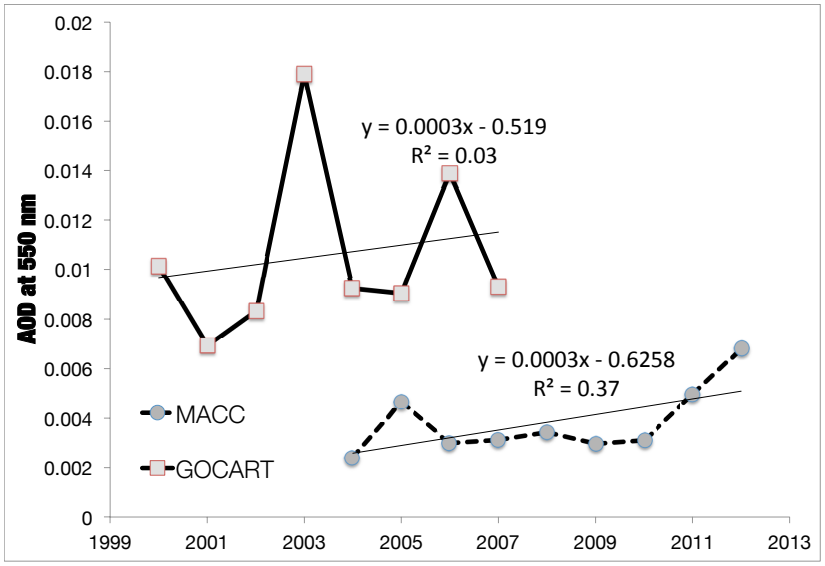
0.02
0.018
0.016
0.014
0.012
0.01
0.008
0.006
0.004
0.002
0
AOD at 550 nm
y = 0.0003x - 0.519
R² = 0.03
y = 0.0003x - 0.6258
R² = 0.37
MACC
GOCART
1999
2001
2003
2005
2007
2009
2011
2013

(b)

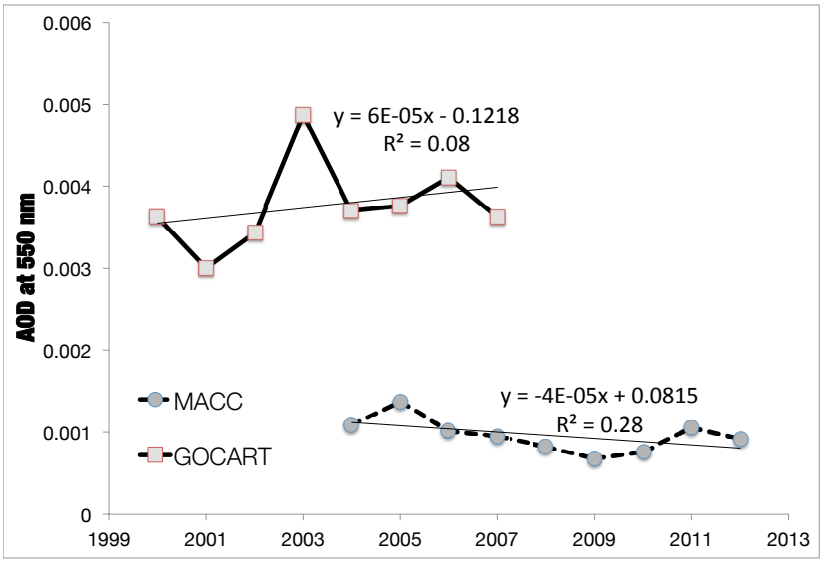

(c)

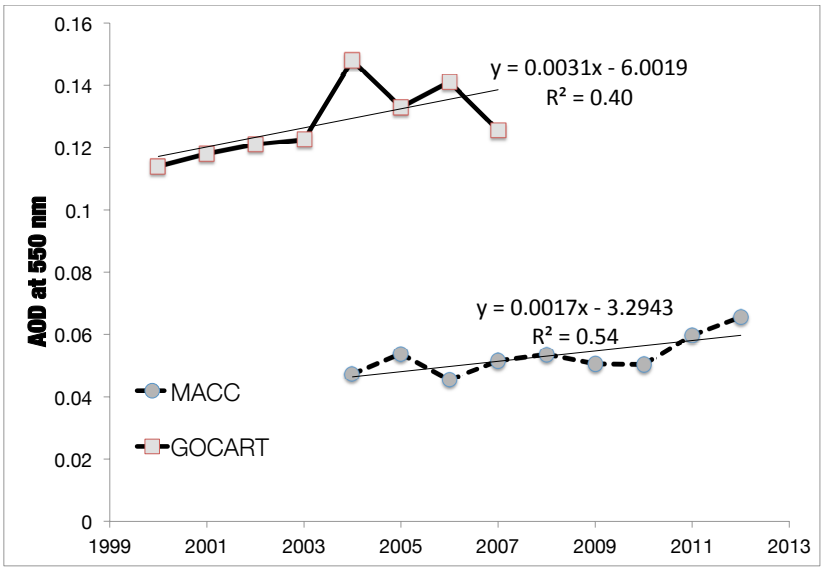

(d)

Figure 13 May – June averaged aerosol optical depth at 550 nm for a) dust, b) organic matter, c) black carbon and d) total obtained from the GOCART model and from the MACC model (as in Dumont et al., 2014) for the domain bounded by 75 to 80°N and 30 to 50° W. All trends are not statistically significant with the exception of the MACC outputs for Dust ($p<0.01$) and Total Aerosol ($p<0.05$).

	STATION		
	Thule 77°28′00″N,69°13′50″W	Ittoqqortoormiit 70°29′07″N, 21°58′00″W	Kangerlussuaq 67°00′31″N, 50°41′21″W
Year			
2007	0.042±0.010	N/A	N/A
2008	0.040±0.017	N/A	0.051±0.012
2009	0.093±0.020	N/A	0.088±0.017
2010	0.052±0.011	0.052±0.005	0.049±0.007
2011	0.060±0.017	0.072±0.041	0.053±0.012
2012	0.065±0.011	0.044±0.009	0.072±0.020
2013	0.050±0.007	0.053±0.009	0.066±0.010

Table *2* June-July-August mean and standard deviation of measured aerosol optical dep
(AOD) at 550 nm at the three sites of Thule, Ittoqqortoormiit and Kangerlussuaq of tl
AERONET network (AERONET web site, http://aeronet.gsfc.nasa.gov, 2013).